JAMES | Journal of Advances in Modeling Earth Systems

RESEARCH ARTICLE
10.1029/2023MS004093

Vertical Structure and Energetic Constraints for a Backscatter Parameterization of Ocean Mesoscale Eddies

Elizabeth Yankovsky[1], **Scott Bachman**[2], **K. Shafer Smith**[1], **and Laure Zanna**[1]

[1]Courant Institute of Mathematical Sciences, New York University, New York, NY, USA, [2]Climate and Global Dynamics Laboratory, National Center for Atmospheric Research, Boulder, CO, USA

Key Points:

- We propose a parameterization for mesoscale eddies targeting ocean models at eddy-permitting resolutions
- We find that both the potential and kinetic energy effects of eddies on the flow may be parameterized via a kinetic energy backscatter
- The novel approach of our backscatter scheme is its use of vertical structure, that is, backscattering onto the equivalent barotropic mode

Correspondence to:
E. Yankovsky,
eyankovsky@gmail.com

Citation:
Yankovsky, E., Bachman, S., Smith, K. S., & Zanna, L. (2024). Vertical structure and energetic constraints for a backscatter parameterization of ocean mesoscale eddies. *Journal of Advances in Modeling Earth Systems*, *16*, e2023MS004093. https://doi.org/10.1029/2023MS004093

Received 24 OCT 2023
Accepted 4 JUN 2024

Abstract Mesoscale eddies modulate the stratification, mixing, tracer transport, and dissipation pathways of oceanic flows over a wide range of spatiotemporal scales. The parameterization of buoyancy and momentum fluxes associated with mesoscale eddies thus presents an evolving challenge for ocean modelers, particularly as modern climate models approach eddy-permitting resolutions. Here we present a parameterization targeting such resolutions through the use of a subgrid mesoscale eddy kinetic energy budget (MEKE) framework. Our study presents two novel insights: (a) both the potential and kinetic energy effects of eddies may be parameterized via a kinetic energy backscatter, with no Gent-McWilliams along-isopycnal transport; (b) a dominant factor in ensuring a physically-accurate backscatter is the vertical structure of the parameterized momentum fluxes. We present simulations of 1/2° and 1/4° resolution idealized models with backscatter applied to the equivalent barotropic mode. Remarkably, the global kinetic and potential energies, isopycnal structure, and vertical energy partitioning show significantly improved agreement with a 1/32° reference solution. Our work provides guidance on how to parameterize mesoscale eddy effects in the challenging eddy-permitting regime.

Plain Language Summary Ocean eddies evolving on horizontal lengthscales of order 10–100 km are not sufficiently resolved in modern global ocean models that have horizontal resolutions of about 25–100 km. The under-representation of such eddies leads to inaccuracies in the modeled ocean state, including weakened current systems, incorrect stratification, and erroneous distributions of physical and biological ocean tracers. Here we develop a novel approach to mimicking the unresolved eddy effects by artificially energizing the flow in a way that is consistent with eddy dynamics, specifically their vertical structure. We find that our approach is able to correct for a variety of unresolved eddy effects when employed in a coarse-resolution ocean model and compared against a high-resolution reference case. Our work provides new insights on how to account for unresolved eddies in the next generation of climate models.

1. Introduction

As modern ocean models approach horizontal grid resolutions that permit the mesoscale range of motion, modelers face new challenges in developing parameterizations for the incompletely resolved mesoscale eddy dynamics (Fox-Kemper et al., 2019; Griffies et al., 2015; Hewitt et al., 2020). The widely-used Gent and McWilliams (hereafter GM) parameterization mimics the effect of baroclinic instability by adiabatically relaxing large-scale lateral buoyancy gradients (Gent et al., 1995; Gent & McWilliams, 1990). The GM scheme successfully parameterizes eddy buoyancy effects in fully non-eddying models but has deleterious effects in eddy-permitting models (Delworth et al., 2012; Henning & Vallis, 2004); here we define the "eddy-permitting" resolution to be near or below the first baroclinic Rossby deformation scale, with some eddy features captured but being only partially resolved. Recently, much work has been aimed at parameterizing the momentum effects of eddies through energy "backscatter" schemes (e.g., Grooms et al., 2015; Jansen & Held, 2014; Juricke, Danilov, Koldunov, Oliver, Sein, et al., 2020; Kitsios et al., 2013; Porta Mana & Zanna, 2014). Owing to under-resolved dynamics and sub-optimal parameterization choices, ocean models are frequently overly-dissipative—harmonic/biharmonic viscosity removes excess kinetic energy from the flow, and due to the incompletely resolved inverse turbulent cascade, the entire wavenumber spectrum is affected (Juricke, Danilov, Koldunov, Oliver, & Sidorenko, 2020; Khani & Dawson, 2023). The use of GM exacerbates this issue in eddy-permitting models (Hallberg, 2013), by damping the partially-resolved eddies and increasing the kinetic energy deficit. On the contrary, backscatter schemes attempt to correct for the over-dissipation by re-energizing the flow (Jansen et al., 2015).

Backscatter alone may also act to relax available potential energy (APE) (Jansen & Held, 2014), further rationalizing its advantage over GM in the eddy-permitting regime.

The premise of parameterizing interactions of the subgrid mesoscale eddy kinetic energy (MEKE) with the resolved flow has gained traction over the last 15 years (Cessi, 2008, Eden & Greatbatch, 2008; Marshall & Adcroft, 2010, among others). Recently, Jansen et al. (2020) introduced a MEKE-based parameterization framework for ocean models that they argue is scale-aware and suitable for resolutions ranging from non-eddying to eddy-resolving. The premise is to solve a 2D prognostic equation for the MEKE, and use the value of MEKE to inform the GM and backscatter coefficients. The MEKE equation is comprised of source terms from viscous dissipation of the resolved state and GM, sink terms due to backscatter and subgrid dissipation, and a subgrid advective term. A parameterization by Bachman (2019) employs a similar approach, assuming that a fraction of the energy extracted by GM is backscattered to the flow. The argument behind both Bachman (2019) and Jansen et al. (2020) is that the dominant energetic balance represented in the subgrid EKE budget is the eddy-driven extraction of APE from the mean flow and its conversion into EKE, which experiences the inverse turbulent cascade and is converted into large-scale, resolved kinetic energy.

A caveat of the Jansen et al. (2020) approach can arise in the eddy-permitting regime, where they propose setting the GM and backscatter coefficients to be equal. In this case, GM can have the unfavorable effect of extracting APE from small-scale flow features, such as eddies, rather than the large-scale buoyancy gradients (see Mak et al. (2023) Figure 1, for a demonstration). Backscatter aims to re-energize these features, causing a double-counting of the APE removal. The solution proposed by Mak et al. (2023) is a flow-splitting procedure that isolates the "large-scale" field to which GM is applied, thus avoiding the eddy damping problem. We develop a second approach here: if an eddy feature is already partially resolved, we will attempt to energize the eddy in such a way that it performs the APE extraction from large scales without the need for GM. We acknowledge that in a realistic GCM these two approaches may eventually be implemented in a complementary manner, though here we focus on purely backscatter-driven isopycnal relaxation. A second caveat lies in the representation of vertical structure. Studies by Juricke et al. (2019); Juricke, Danilov, Koldunov, Oliver, and Sidorenko (2020) have explored the use of a 3D MEKE budget to allow for representation of vertical fluxes, though a 3D budget is computationally expensive and necessitates theoretical guidnace on the formulation of vertical fluxes. The Jansen et al. (2020) scheme uses a 2D, vertically averaged MEKE field for informing the antiviscosity of the backscatter. However, in situations where the flow is already too baroclinic due to under-resolved eddy vertical fluxes and barotropization, this approach will only maintain or heighten the erroneous vertical structure of the flow. Constraining the vertical structure of subgrid eddy fluxes for backscatter parameterizations remains an open challenge.

Here we propose parameterizing mesoscale eddies through kinetic energy backscatter without the use of GM in an effort to avoid the aforementioned negative effects of GM at eddy-permitting resolutions. We show that both the kinetic and potential energy effects of unresolved mesoscale eddies on the resolved flow may be parameterized by a correctly formulated backscatter term. The key component maintaining energetic consistency in our backscatter parameterization is imposing an equivalent barotropic vertical structure onto the backscatter antiviscosity, computed using a 2D MEKE budget. We retain a 2D budget to avoid the additional degrees of freedom in parameterizing inter-layer fluxes, computational expense, and implementation challenges of a 3D budget. Instead, 3D structure is incorporated via a depth-dependent backscatter antiviscosity, based on the equivalent barotropic dynamical mode that is representative of EKE vertical structure (de La Lama et al., 2016).

We employ the idealized model NeverWorld2 (Marques et al., 2022) as a testbed for developing our backscatter scheme. The paper begins by providing details of the NeverWorld2 configuration, the parameterization formulation, and the process of how and why we developed this scheme. We then compare the results of a high-resolution (1/32°) reference simulation, an unparameterized low-resolution (1/2°) simulation, a 1/2° simulation with our backscatter scheme, and a 1/2° simulation using the Jansen et al. (2020) approach of equally tuned GM and backscatter. Mean and eddy flow metrics related to the buoyancy and energetic structure of the simulations will be compared to assess the performance of our backscatter scheme. Finally, we discuss limitations and new questions that the scheme raises and end with conclusions.

2. A Testbed for Eddy Parameterization Development

To develop and validate our parameterization, we have employed the NeverWorld2 (NW2) model detailed in Marques et al. (2022). NW2 is an adiabatic, stacked shallow water configuration of the GFDL-MOM6. It

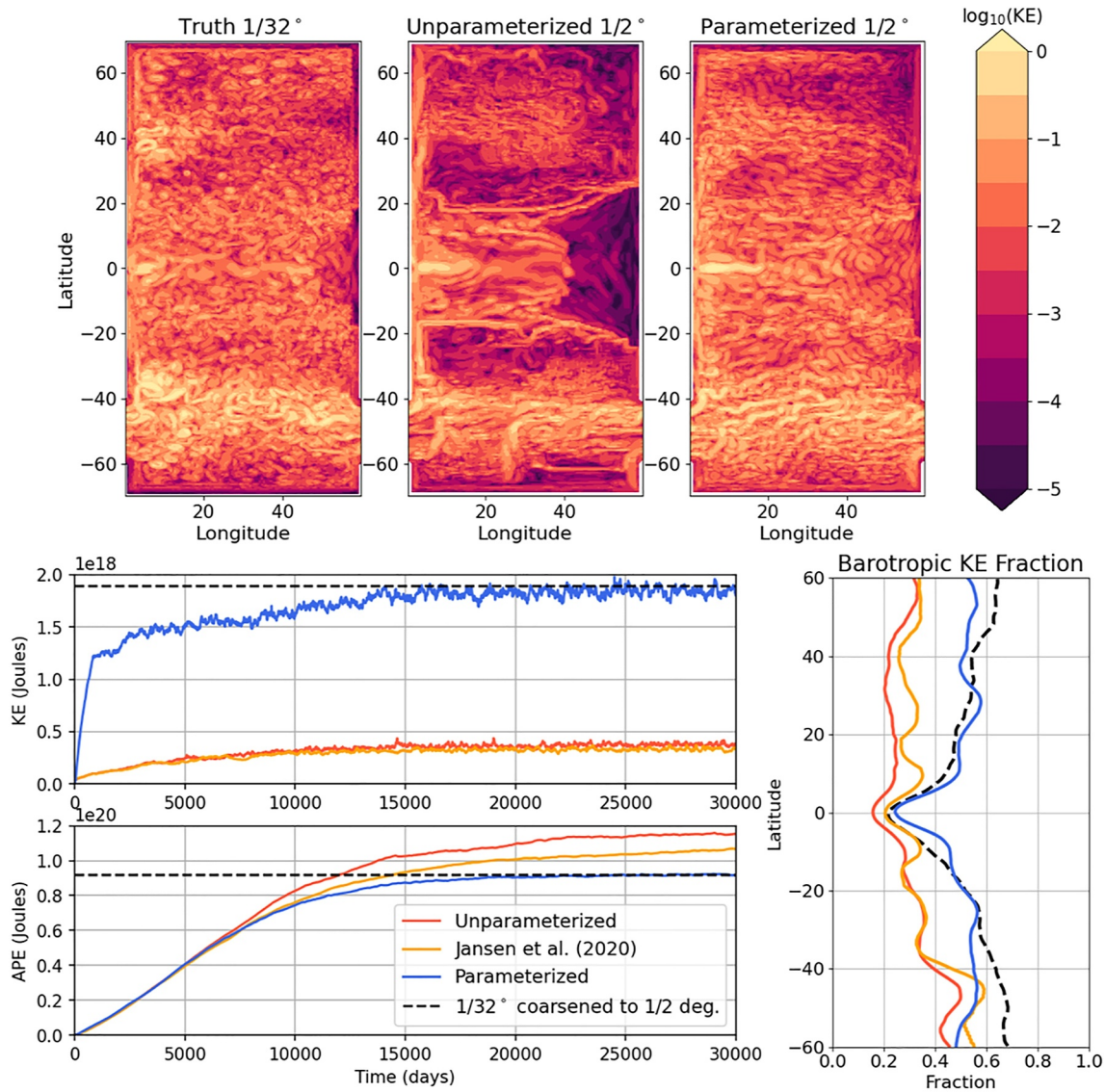

Figure 1. Upper row: 5-day averaged surface kinetic energy on a logarithmic scale for a high-resolution (1/32°) reference simulation, a low-resolution (1/2°) simulation with no eddy parameterization, and a low-resolution (1/2°) simulation with our backscatter scheme. The 1/2° simulation using the Jansen et al. (2020) scheme looks nearly identical to the unparameterized case when considering the surface KE (not shown). Lower left: timeseries of globally integrated kinetic and available potential energy for the 1/2° unparameterized case, the Jansen et al. (2020) and our backscatter parameterizations, and the reference simulation's steady-state values coarsened onto a 1/2° grid. Lower right: zonally-averaged values of the fraction of kinetic energy in the barotropic mode of the flow for the same simulations.

represents a two-hemisphere idealization of the Atlantic Ocean, with a topographic ridge extending through the middle of the domain and a channel representing the Southern Ocean in the southern hemisphere. The model is forced only by a meridionally-varying, temporally constant wind. As such, the model provides a well-tailored means by which to study and parameterize ocean eddies driven by baroclinic instability, whose physics are predominantly adiabatic.

Prior works (e.g., Kjellsson and Zanna (2017) in a realistic global model, Yankovsky et al. (2022) in the idealized NW2), have considered how the representation of mesoscale eddies changes as a function of resolution and what effects under-resolved eddies have on the resolved flow. A main finding of these studies is that the vertical structure of the flow becomes increasingly baroclinic as the model resolution is coarsened. The vertical eddy energy fluxes that lead to barotropization (Chemke & Kaspi, 2016; K. S. Smith & Vallis, 2001) are not fully captured at eddy-permitting resolutions. Additionally, as resolution is coarsened the APE of the flow becomes

higher and the KE lower. We hypothesize that these issues may be mediated by the use of a backscatter with vertical structure representing that of EKE in a high-resolution model.

In Marques et al. (2022) and Yankovsky et al. (2022) we considered a hierarchy of four horizontal resolutions of NW2: 1/4°, 1/8°, 1/16°, and 1/32°. The 1/32° was taken as the "truth" and lower resolutions were compared against it. The most fundamental shift in flow properties occurred between the 1/4° and 1/8° resolutions. The 1/8° and higher resolution models all had similar vertical flow structure; the main difference was the kinetic energy of the flow. By contrast, at 1/4° the baroclinic Rossby radius is unresolved over most of the domain and the flow vertical structure is significantly more baroclinic than the higher resolutions. Although eddies are present and grid spacing is close to the deformation radius, the inverse energy cascade driven by eddies is unresolved. A study by Loose et al. (2022) also considered scale-dependent energetics in the NW2 model as a basis for developing scale- and flow-aware parameterizations particularly for eddy-permitting models. For NW2 (and ocean models more broadly), we consider the eddy-permitting resolution to begin roughly at 1/2° to 1/4°. We will thus focus on the 1/2° case—the more challenging limit as it is barely eddy-permitting—when developing and testing our parameterization.

We will discuss the details of our parameterization below, but we begin with a demonstration of our scheme's performance. Figure 1 shows an overview of how our parameterization compares against the Jansen et al. (2020) scheme and an unparameterized simulation at 1/2° resolution as well as the high-resolution "truth" case (1/32°). The surface KE in the truth case shows a richly eddying structure throughout the domain. The highest energies are seen in the Southern Ocean, where wind stress is largest, as well as in the western boundary current region in the northern hemisphere. The unparameterized 1/2° simulation is significantly less energetic, noting that the figure uses a logarithmic color scale. There are zones where the energy is nearly three orders of magnitude smaller than the truth case, such as in the midlatitudes, eastern low latitudes, and northernmost part of the domain. Additionally, due to the constant-in-time wind forcing and lack of resolved eddies, there are unphysical zonal bands of high energy. The 1/2° simulation using the Jansen et al. (2020) scheme (not shown in the upper panel) looks nearly identical to the unparameterized case when considering the surface KE distribution. In our parameterized 1/2° simulation, we see a remarkable improvement in the surface energy levels and structure. The zonal features arising in the unparameterized case are no longer evident and the energy levels are comparable to that of the truth case. The Southern Ocean and western boundary current regions also have better resemblance with the truth case. The globally integrated kinetic and potential energy for the same three cases and the Jansen et al. (2020) case are shown in the bottom of Figure 1. The 1/2° case with our parameterization has a global APE and KE that is nearly identical to that of the truth case coarsened onto a 1/2° grid, whereas the unparameterized case has overly high APE and a KE nearly an order of magnitude smaller. The Jansen et al. (2020) case has roughly the correct APE, about 10% higher than the truth (this can be improved via tuning). The main issue is that the KE is nearly the same as the unparameterized case. Finally, the vertical structure of the flow with our parameterization on is substantially improved relative to the unparameterized and Jansen et al. (2020) cases. We see a much larger portion of the KE in the barotropic part of the flow, in line with the truth case.

3. Parameterization Formulation

The equations in this section will be presented in a Cartesian frame for simplicity, but can be readily generalized to other vertical coordinate systems using appropriate transformations and metric coefficients (e.g., Griffies (2004)). The vector-invariant momentum equation is

$$\frac{\partial \mathbf{u}}{\partial t} + (f+\zeta)\,\hat{\mathbf{z}}\times\mathbf{u} + \nabla(K+M) = \frac{1}{\rho_0}\frac{\partial \boldsymbol{\tau}}{\partial z} - \nabla\cdot\left[\nu_4\nabla^2\dot{\mathbf{s}}\right] + \nabla\cdot\left[\nu_2\dot{\mathbf{s}}\right], \tag{1}$$

where

$$\dot{\mathbf{s}} = \begin{bmatrix} \sigma_T & \sigma_S \\ \sigma_S & -\sigma_T \end{bmatrix} \tag{2}$$

is the trace-free part of the strain rate tensor (the symmetric part of the velocity gradient tensor). Here, $\mathbf{u} = (u, v)$ is the horizontal velocity vector, $f = 2\,\Omega\sin\theta$ is the Coriolis parameter (with $\Omega = 7.2921\times10^{-5}$ s^{-1} and latitude

θ), $\zeta = \frac{\partial v}{\partial x} - \frac{\partial u}{\partial y}$ is the vertical component of the relative vorticity, $\sigma_T = \frac{\partial u}{\partial x} - \frac{\partial v}{\partial y}$ is the horizontal tension, $\sigma_S = \frac{\partial v}{\partial x} + \frac{\partial u}{\partial y}$ is the shearing strain, $\hat{\mathbf{z}}$ is the unit vector in the vertical direction, and $\nabla = \left(\frac{\partial}{\partial x}, \frac{\partial}{\partial y}\right)$ is the horizontal gradient. The kinetic energy density is K, Montgomery potential is M, and $\frac{1}{\rho_0}\frac{\partial \boldsymbol{\tau}}{\partial z}$ is the wind forcing. The second-to-last term is a biharmonic dissipation, where ν_4 is set using the Smagorinsky scheme (Griffies & Hallberg, 2000),

$$\nu_4 = \left(c_{\text{smag}}\sqrt{\left(\frac{\partial u}{\partial x} - \frac{\partial v}{\partial y}\right)^2 + \left(\frac{\partial u}{\partial y} + \frac{\partial v}{\partial x}\right)^2}\right)\Delta^4, \tag{3}$$

with $c_{\text{smag}} = 0.2$ (Marques et al., 2022) and Δ is horizontal grid spacing. The last term in (Equation 1) is the backscatter, formulated as a harmonic antiviscosity, and the form of its coefficient ν_2 shapes the eddy parameterization. Following Jansen et al. (2020).

$$\nu_2 = c\sqrt{2e}L_{\text{mix}}, \tag{4}$$

where c is a nondimensional tuning parameter that is negative for backscatter, $e = e(x, y, t)$ is vertically-averaged subgrid Mesoscale Eddy Kinetic Energy (MEKE), and L_{mix} is the subgrid-scale mixing length set as the minimum of the grid spacing and the generalized Rhines scale $L_{\beta^*} = (2e)^{1/4}\beta^{*-1/2}$. The topographically modified barotropic planetary vorticity gradient is $\beta^* = \left|\frac{\partial f}{\partial y}\hat{\mathbf{y}} - f\nabla H/H\right|$, with local ocean depth H.

Subgrid MEKE is set using a local dynamic budget proposed by Jansen et al. (2020),

$$\frac{\partial e}{\partial t} = \dot{e} = \dot{e}_{\text{GM}} + \dot{e}_{\text{Smag}} - \dot{e}_{\text{BScat}} - \dot{e}_{\text{diss}} - \dot{e}_{\text{adv}}. \tag{5}$$

There are two source terms of subgrid EKE. The first is $\dot{e}_{\text{GM}}$, determined by the rate at which a GM parameterization (if used) converts potential energy (PE) from the resolved flow to EKE through buoyancy diffusion. The second, $\dot{e}_{\text{Smag}}$, has momentum source $\nabla \cdot \left[\nu_4 \nabla^2 \dot{\mathbf{s}}\right]$, and captures the rate at which biharmonic Smagorinsky viscosity extracts KE from the resolved flow. The sinks of subgrid EKE are: the backscatter of EKE into the resolved flow implemented via the harmonic antiviscosity term, $\dot{e}_{\text{BScat}}$ (with momentum sink $\nabla \cdot \left[\nu_2 \dot{\mathbf{s}}\right]$), and $\dot{e}_{\text{diss}}$, the subgrid frictional dissipation of EKE in the bottom boundary layer, parameterized using a quadratic drag law. The last term in (Equation 5) is the horizontal transport of subgrid EKE parameterized via diffusion and advection by the resolved barotropic flow, and should integrate to zero over the domain. For further details see Jansen et al. (2020).

Note that all terms in Equation 5 are 2D. A novel component of the parameterization presented here is the imposition of vertical structure in the antiviscous coefficient, so that $\nu_2 = \nu_2(z)$. Through a great deal of experimentation, we found that to improve the fidelity of parameterized simulations, two aspects of its vertical structure were particularly important: its amplitude should be surface-intensified, and vanish at the ocean's floor. This is consistent with an analysis of moored current meters by de La Lama et al. (2016), showing that the ocean's kinetic energy projects strongly onto the Equivalent Barotropic Mode (EBT), and further buttressed by theoretical arguments that this is consistent with the effects of rough bottom topography on EKE (LaCasce, 2017). We leverage this result in our parameterization; although we do not explicitly resolve the vertical energy fluxes driven by ocean eddies, we parameterize the expected end state in which the EKE has a vertical structure that is well-approximated by the EBT mode.

The EBT mode arises from the eigenvector problem for the quasigeostrophic stretching operator,

$$\frac{d}{dz}\left(\frac{f^2}{N^2}\frac{d\phi_j}{dz}\right) + \lambda_j^2 \phi_j = 0. \tag{6}$$

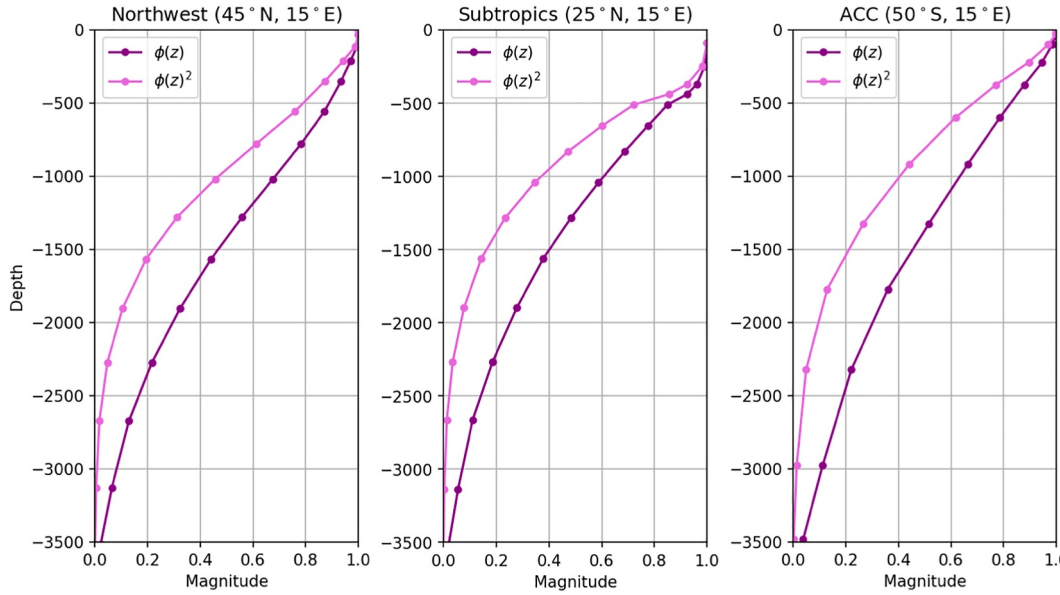

Figure 2. EBT mode structure at three locations within the NW2 domain—Northwest, subtropics, and Antarctic Circumpolar Current. The EBT mode as derived above is for the horizontal velocity structure; we additionally plot the square of the EBT mode to reflect the vertical structure of the kinetic energy. Note that the above EBT mode structures were computed for a coarse-resolution 1/2° NW2 configuration (consistent with the higher resolution cases, not shown).

Here f is the Coriolis parameter, $N(z)$ is the buoyancy frequency, $\phi_j(z)$ are the eigenvectors, and λ_j^2 are the associated eigenvalues, with $j = 0, 1, 2\ldots$. The traditional baroclinic modes are the eigenvectors that arise with Neumann boundary conditions at the surface and bottom, that is, $\frac{d\phi}{dz} = 0$ at $z = 0, -H$. In this case $\lambda_0 = 0$, and $\phi_0(z) = 1$ is the standard barotropic mode, equivalent to a depth-average. If one instead uses a Neumann condition at the top and a Dirichlet condition at the bottom, that is,

$$\left.\frac{d\phi}{dz}\right|_{z=0} = 0 \quad \text{and} \quad \phi|_{z=-H} = 0, \tag{7}$$

one finds that the first eigenvalue $\lambda_0 \neq 0$, and the first eigenvector $\phi_0(z)$ is depth-dependent, with a surface-intensified structure and a vanishing amplitude at the bottom (LaCasce & Groeskamp, 2020; K. Smith & Vanneste, 2013). $\phi_0(z)$ is the EBT mode, hereafter denoted simply $\phi(z)$.

We obtain the EBT mode's vertical structure by numerically solving (Equation 6) using the local buoyancy frequency with rigid lid surface and Dirichlet bottom boundary conditions. The resulting $\phi(z)$ is plotted for three sample locations in Figure 2. Assuming $\phi(z)$ reflects the structure of eddy horizontal velocity, then its square, also shown, corresponds to the vertical structure of EKE. In our parameterization scheme, we set the backscatter antiviscosity coefficient as

$$\nu_2 = \phi(z)^2 c\sqrt{2e}L_{\text{mix}}. \tag{8}$$

Note that we raise the EBT mode to the second power. If we were to follow the traditional mixing length theory, then we should have $\nu_2(z) = \sqrt{\phi(z)^2 e}\, L_{\text{mix}}$, and the EBT mode should be raised to a power of one. We did test this approach, but it led to too much removal of APE (not too surprising, as the mixing length argument is an idealization). We used a power of two for empirical reasons, as it creates a more surface-intensified backscatter and increases fidelity compared to the high-resolution case. We admit that further exploration into the vertical structure based on resolution and flow dynamics is warranted, please see the discussion. The advantage of relying on the EBT mode is that it is already implemented in MOM6 via a tridiagonal solver and is computationally

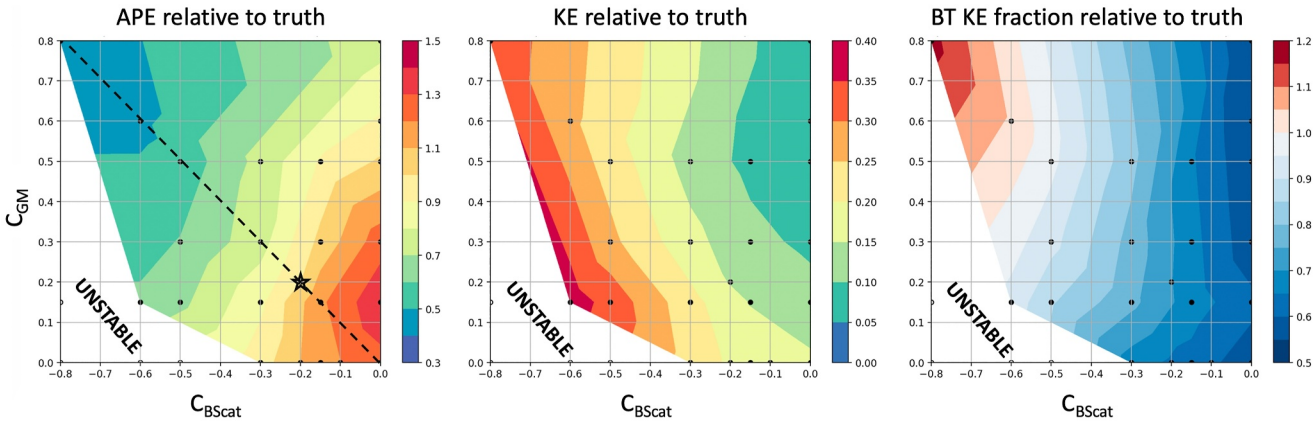

Figure 3. Here we consider three metrics—globally integrated available potential energy (APE) and kinetic energy (KE), as well as globally averaged barotropic KE fraction. The metrics are computed for a suite of 1/2° simulations using the Jansen et al. (2020) scheme, varying the tuning coefficient before the Gent-McWilliams (c_{GM}) and backscatter (c_{BSat}) terms. They are then divided by the value of the same metric for the reference 1/32° simulation coarsened onto a 1/2° grid, so that a value of 1.0 represents a simulation that is in line with the reference solution. The dashed line shows the Jansen et al. (2020) approach of choosing $C_{GM} = -C_{BScat}$, with the star indicating the tuning corresponding to the closest APE to the truth (their criterion for choosing the coefficient magnitude).

inexpensive. Alternative formulations for ν_2 and their consequences are also considered in Section 4 and the appendix.

The final novel component of our scheme is the use of a technique to stabilize the backscatter. The premise of using a biharmonic operator to dissipate energy and a harmonic (Laplacian) operator to backscatter energy is to attempt to return energy to the flow at larger scales than it is being removed (Jansen & Held, 2014). In practice, however, this approach can lead to numerical instability. In some instances, $\dot{e}_{\mathrm{BScat}}$ can locally inject energy into the resolved flow faster than $\dot{e}_{\mathrm{Smag}}$, $\dot{e}_{\mathrm{adv}}$, and $\dot{e}_{\mathrm{diss}}$ can remove it. We have therefore formulated a criterion for avoiding such instability by implementing a backscatter shutoff when the dissipation term $\dot{e}_{\mathrm{Smag}}$ reaches a threshold value. This technique is described in greater detail in Section 4. For further details on the terms of the MEKE budget, see Jansen et al. (2020) and references therein. For further details on the development of our scheme and an alternative formulation for the antiviscosity, see Section 4 and the appendix.

4. Why Impose Vertical Structure on the Backscatter?

Prior to examining the results from our scheme, we dedicate a section to addressing how and why we realized that vertical structure is critical to ensuring a physically accurate backscatter. We will discuss sensitivity experiments using the Jansen et al. (2020) approach and the steps that led to the development of our scheme. Numerous prior works have focused on incorporating vertical structure into the GM and Redi diffusivities. Ferreira et al. (2005) proposed a horizontal eddy diffusivity with a surface intensification, suggestive of a dependence on the stratification N^2. Ferrari et al. (2010) constructed a mesoscale eddy-induced transport streamfunction to have a low baroclinic mode vertical structure and to smoothly transition through regions of weak stratification such as boundary layers or mode waters. Zhang and Wolfe (2022) investigated the vertical structure of the anisotropic along-isopycnal diffusivity. These works point to the vertical structure being similarly important for kinetic energy backscatter parameterizations.

However, interestingly, we began this work not with the intent of adding a vertical structure into the backscatter. Rather, we were testing both the Bachman (2019) and Jansen et al. (2020) schemes in the NW2 model and investigating how to optimally tune the GM and backscatter components for an eddy-permitting model. We first asked: should we tune the GM and backscatter components with the same tuning constant as suggested by Jansen et al. (2020)? Is it advantageous to rely more on GM, more on backscatter, or a combination of the two? Through the process of answering these questions, we rediscovered the importance of vertical structure in ensuring energetic fidelity of our parameterized solution. We next describe how we came to this realization.

We began by performing a parameter sweep across variable GM and backscatter tuning constants in the 1/2° NW2 (Figure 3). We computed the global APE, KE, and average barotropic KE component of the coarsened reference

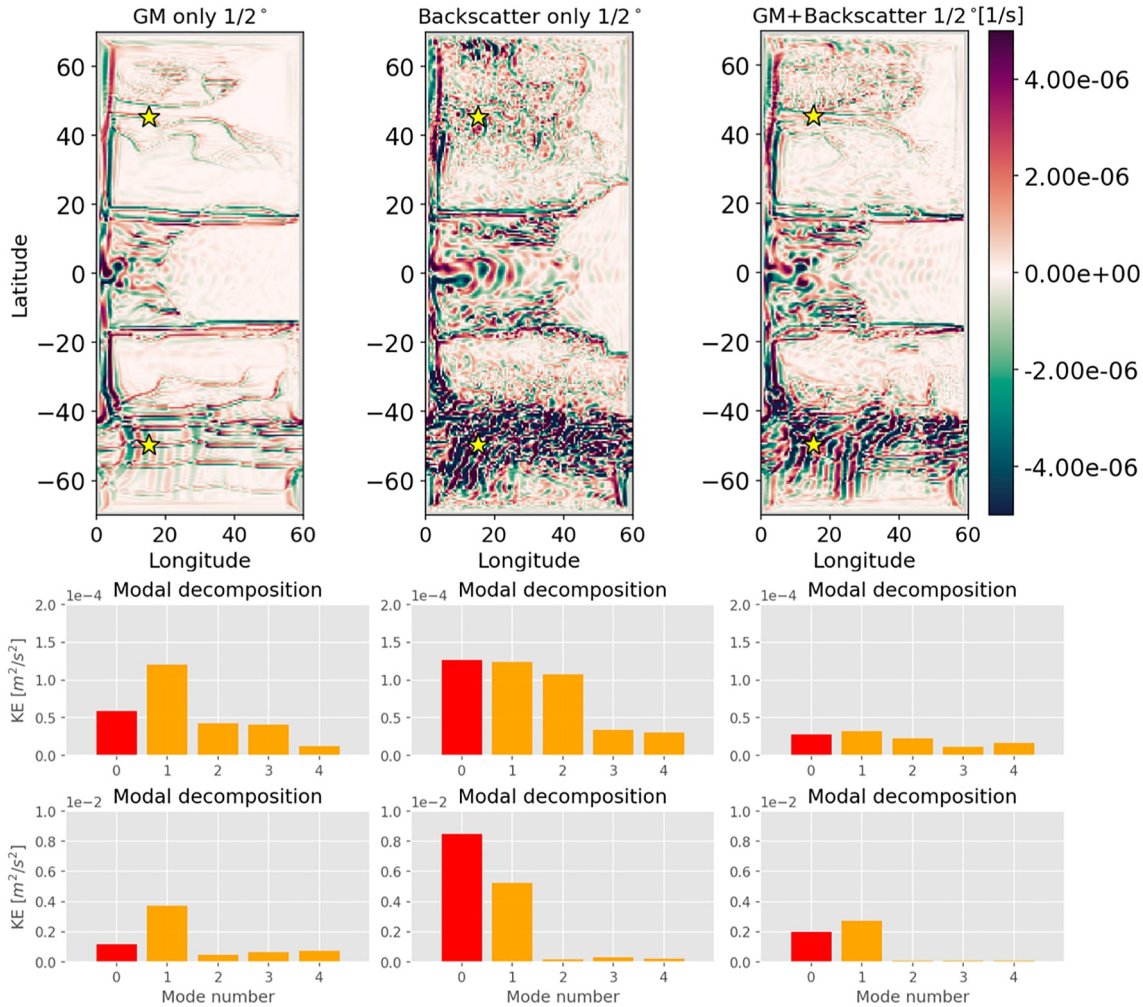

Figure 4. Comparison of 5-day averaged surface relative vorticity (top panel), and 500-day averaged kinetic energy decomposition into vertical modes (see also the later Figures 10 and 11) for the two starred locations shown in the top panel. Middle row is for the northern location and lower row is for the southern location. Note that the zeroth mode refers to the barotropic mode. The left column uses only the Gent-McWilliams component of the Jansen et al. (2020) scheme, middle uses only the backscatter component of Jansen et al. (2020) (with no vertical structure), and the right uses the default Jansen et al. (2020) setup with both GM and backscatter with equal tuning coefficients.

simulation and compared it against the 1/2° simulations with varying GM and backscatter coefficients (C_{GM} and C_{BScat}). Note that Jansen et al. (2020) propose tuning the GM constant by matching the global APE to the reference, and then imposing the same tuning constant for backscatter (shown as the star in the figure). Interestingly, though the APE decreases with increasing GM (as expected), it shows a stronger sensitivity to the backscatter coefficient C_{BScat}. The KE and barotropic KE component are also more sensitive to backscatter rather than GM coefficient. If we extrapolate the trends evident in Figure 3, to obtain APE, KE, and barotropic KE fraction values closest to that of the reference, GM should be turned off/minimal and C_{BScat} should be significantly larger in magnitude than what is currently achievable due to stability issues. For values of the backscatter tuning coefficient larger in magnitude than -0.3, the simulation becomes unstable. The simulation closest to the reference that we were able to achieve stability for (prioritizing APE) had $C_{GM} = 0$, $C_{BScat} = -0.3$, and here the KE was only about a third of the reference case and overly baroclinic.

In Figure 4 we examine the surface relative vorticity and decomposition of KE into vertical modes for simulations using the Jansen et al. (2020) scheme with GM only, backscatter only, and equally tuned GM and backscatter. Although none of the simulations have the correct vertical energy partitioning with barotropization accurately captured (see the later Figures 10 and 11 for the reference case), we see the most resemblance in the relative vorticity field of the backscatter-only case when compared against the reference solution. Further, the backscatter-

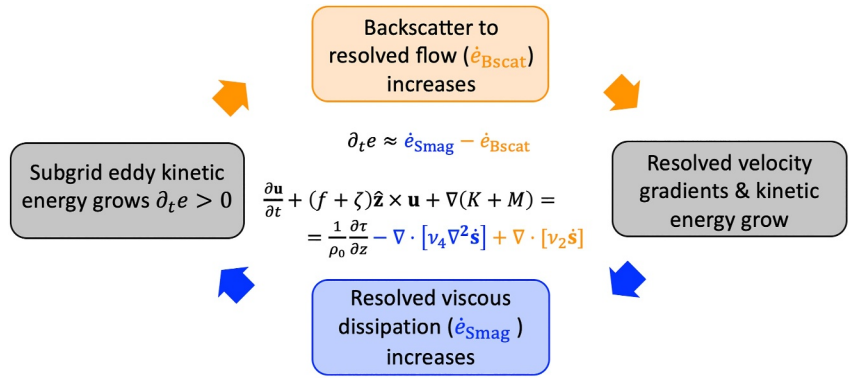

Figure 5. Diagram showing the feedback loop that can lead to instability in the backscatter parameterization. The feedback occurs when the backscatter (having a harmonic operator) and viscous dissipation prescribed in the model (here a Smagorinsky scheme with a biharmonic operator) have little scale separation in a particular region of the flow or eddy feature. The two operators act on the same region, causing a rapid increase in energy and extreme velocities; the CFL condition is violated and the model blows up.

only case preserves the largest amount of KE in the barotropic part of the flow. Both the GM and GM with backscatter cases are overly baroclinic, have very little eddy activity, and have lower overall KE. Given the fact that the global APE, isopycnal structure, KE, and barotropization in the eddy-permitting NW2 was best captured with backscatter alone, we became motivated to explore methods to stabilize the backscatter while turning off GM. The instability in the backscatter involved isolated eddy features that were becoming over-energized, eventually leading to flow velocities of tens of meters per second and violating the CFL criterion.

Figure 5 summarizes our hypothesis for what causes the backscatter to become numerically unstable. As will be later shown in Figure 13, the dominant energy balance in the subgrid EKE budget is between the backscatter sink and viscous source terms. The same two terms are present in the momentum equation (Equation 1) of the resolved flow as an antiviscosity and viscosity (respectively). In some instances, an eddy feature having high subgrid EKE and thus a high backscatter amplitude falls into a feedback cycle where the backscatter and dissipation both grow in magnitude. The viscous dissipation is unable to remove energy as quickly as it is being put in by the backscatter and the velocities within the eddy feature become extreme, leading to numerical instability. We circumvented this feedback loop by implementing a backscatter shutoff based on a viscous CFL criterion. Within the GFDL-MOM6 there is a CFL limit on how large the biharmonic viscosity ν_4 may be (given by Δ^4/dt, where Δ is grid spacing and dt is time step). When ν_4 reaches 1/4 of this limit, we modify the subgrid EKE budget by removing the viscous source term and shutting off backscatter:

$$\frac{\partial e}{\partial t} = -\dot{e}_{\mathrm{diss}} - \dot{e}_{\mathrm{adv}}. \tag{9}$$

The use of a value of 1/4 is somewhat empirical, we found this value to be restrictive enough to prevent numerical instability but not too restrictive in turning off the backscatter. Note that we also attempted decreasing the time step to reduce instability; this partially helped but was not sufficient. Since decreasing the time step incurs additional computational cost, we opted to keep the time step the same as the reference simulation and pursue the stabilizing method described prior.

With only this modification to the Jansen et al. (2020) scheme, we were able to increase the backscatter coefficient so that the KE became comparable to that of the high-resolution reference case without instability. Though the KE magnitude was in agreement with the reference solution, we realized that the global APE was significantly too low—roughly half that of the reference solution. In other words, the backscatter without vertical structure was causing too much dissipation and leading to erroneous isopycnal structure. At this point, we hypothesized that incorporating a vertical structure for the backscatter antiviscosity $\nu(z)$ may be a solution. We tested several choices for modulating ν_2 by a vertical structure (not shown in the figures). We first hypothesized that the best way to parameterize eddy vertical structure effects would be to consider the "final" part of the turbulent energy cascade—the inverse cascade of energy in the barotropic mode. We implemented a barotropic version of the

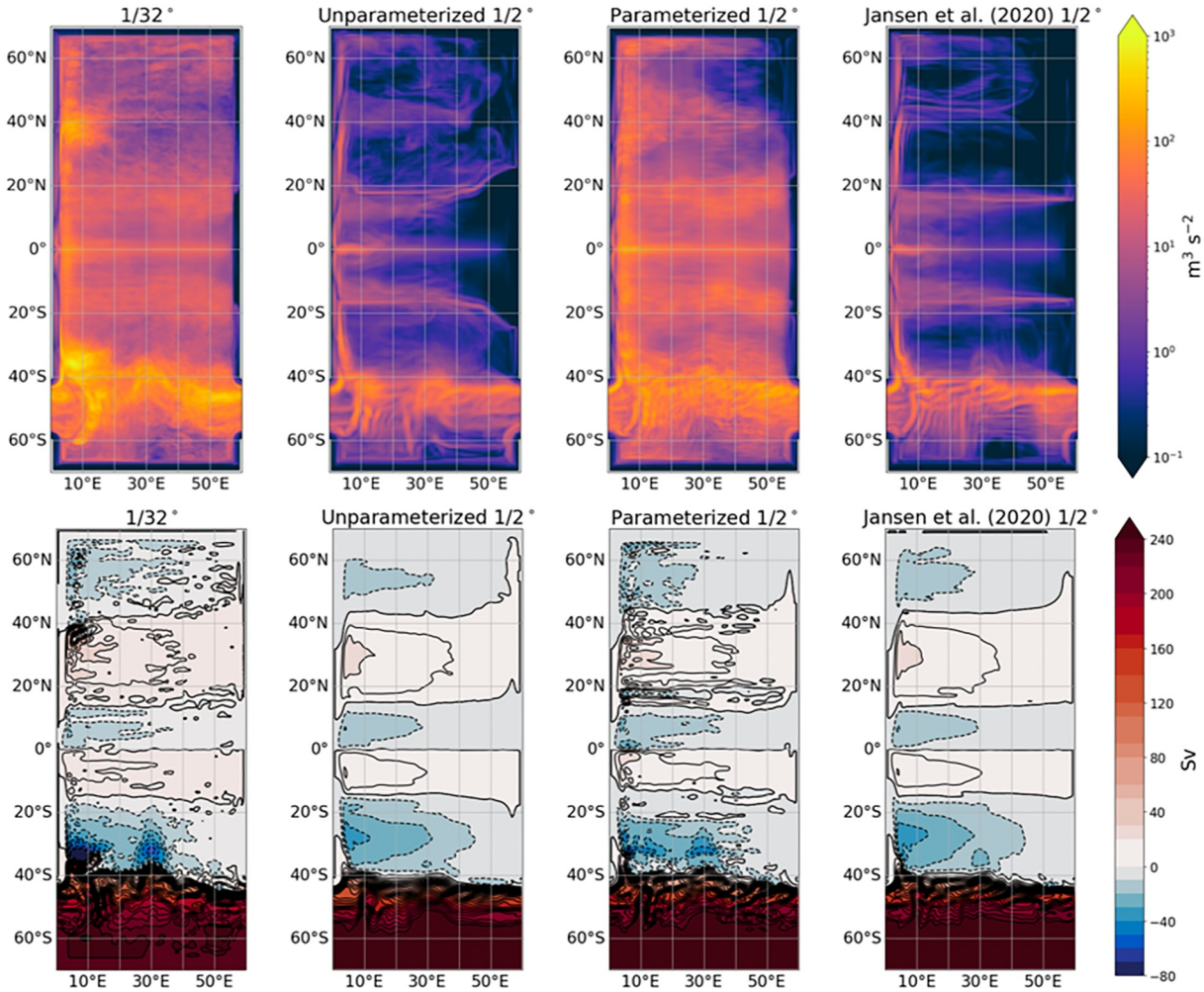

Figure 6. Top row: Depth-integrated kinetic energy averaged over the last 500 days of each simulation. Bottom row: Time-mean barotropic transport stream function (Sv) averaged over the last 500 days of each simulation. Simulations shown are (left to right): reference (1/32°), unparameterized 1/2°, 1/2° with our parameterization, and 1/2° with the Jansen et al. (2020) scheme. For analogous figures for each of the NW2 resolutions, please see Marques et al. (2022), Figures 7 and 10.

backscatter and tuned it such that the global KE matched that of the reference simulation. Note this is similar to the Jansen et al. (2020) case, except for the inclusion of our stabilizing technique (which allowed us to tune the KE to match that of the reference case). Interestingly, the APE of this simulation was again significantly too low. We hypothesize that due to energy re-injection near the bottom, energy is removed through the bottom drag. We then tested a first baroclinic modal structure (using flat bottom modes); again due to the nonzero magnitude near the bottom, we found that too much APE was being removed from the flow. We switched to a constant e-folding decay scale with depth (testing values of 500 and 700 m), which substantially improved the solution and motivated us to try the EBT mode (which similarly decays to a zero value near the bottom). This proved to be an appropriate choice; when we tuned this case so that the KE matched that of the truth case, the APE also perfectly matched. Note that we ended up using the EBT mode squared in Equation 8, a somewhat empirical choice to ensure that backscatter magnitude falls off to zero near the bottom.

We then explored whether the functional form of the antiviscosity affects the performance of the parameterization. We tested a second approach which has a different scaling for the antiviscosity $\nu_2(z)$, but retains the same EBT vertical structure. The alternative scaling has the form:

$$\nu_2(z) = c\frac{2e}{||\dot{\mathbf{s}}||}\phi^4(z), \tag{10}$$

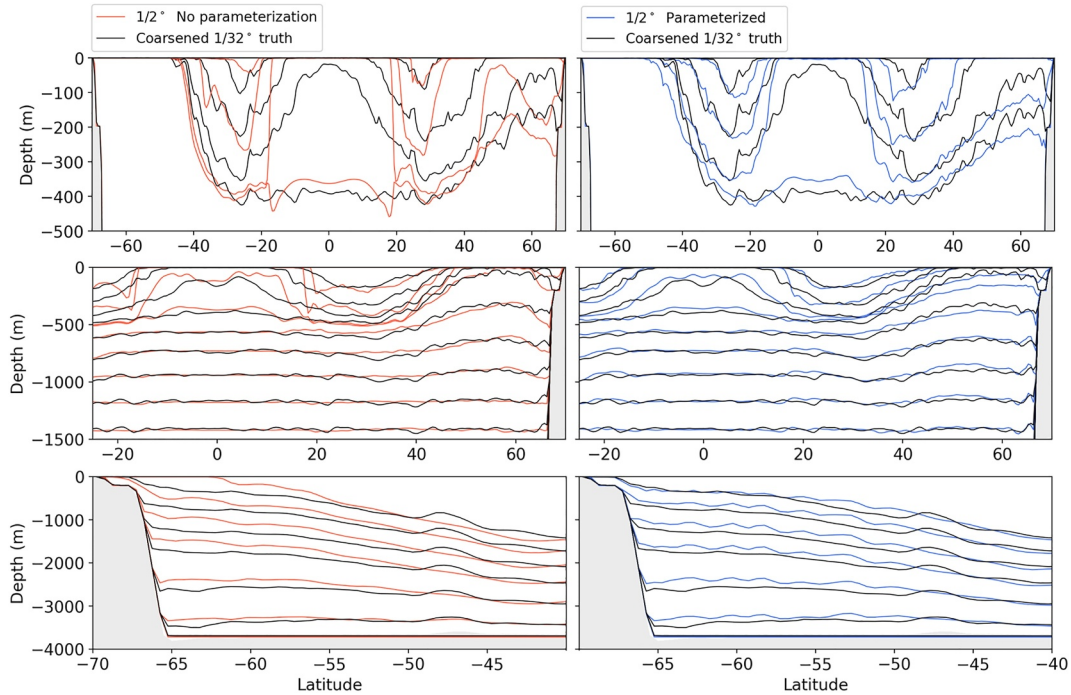

Figure 7. Left column: 500-day averaged isopycnal positions for the 1/2° simulation with no eddy parameterization. Right column: same, for 1/2° simulation with our backscatter scheme. Top row is the upper 5 isopycnals through 45° longitude, middle row shows the upper 1,500 m at 15° longitude, and lowest row shows lowest 6 isopycnals in the Southern Ocean at 45° longitude. In all plots, black lines show the coarsened reference (1/32°) simulation's isopycnal positions.

where $\|\cdot\|$ is the tensor norm operator. This approach is based on deriving the theoretical upper bound on the antiviscosity (see Appendix A for the derivation). This scaling has a linear relationship between the eddy energy and antiviscosity. The linear relationship between eddy energy and diffusivity, where viscosity may be thought of as a momentum diffusivity, has its origins in the approach used in the GEOMETRIC mesoscale eddy parameterization (Mak et al., 2018, 2022; Marshall et al., 2012). For consistency with Equation 8 we raise the power of the EBT mode to 4, since we found that the power of 2 best represents the vertical structure of the square root of the EKE. Remarkably, we found that the two approaches produce nearly identical results. This further emphasizes that the crucial piece of the backscatter parameterization is having a decaying vertical structure. To summarize, after stabilizing the backscatter we found multiple approaches that would yield KE values identical to that of the reference. The challenging part was having KE and APE values simultaneously matching up to the reference; this was only accomplished by choosing the appropriate vertical structure in our backscatter antiviscosity.

5. Evaluating Our Parameterization

We now evaluate a suite of metrics for a 1/2° simulation with and without our parameterization turned on. The metrics will be compared against a 1/32° reference solution. For some metrics we will additionally show the results from a 1/2° simulation employing the Jansen et al. (2020) scheme in its default configuration with GM and backscatter active. We begin by considering the effects on the mean flow and then consider how eddy variability, energy, structure, and scale are influenced by our backscatter parameterization.

5.1. Mean Flow Influences

As observed in Figure 1, and described in the prior section, the major achievement of our parameterization is that the global APE and KE of the parameterized case are simultaneously consistent with the reference case through the use of backscatter alone. We next ask whether local properties over the model domain are similarly consistent. We identify the same mean flow metrics considered in Section 4 of Marques et al. (2022) to evaluate the performance of our parameterization. We begin by considering the depth-integrated KE averaged over 500 days and the time-mean barotropic transport streamfunction to asses the mean state. These metrics are presented in

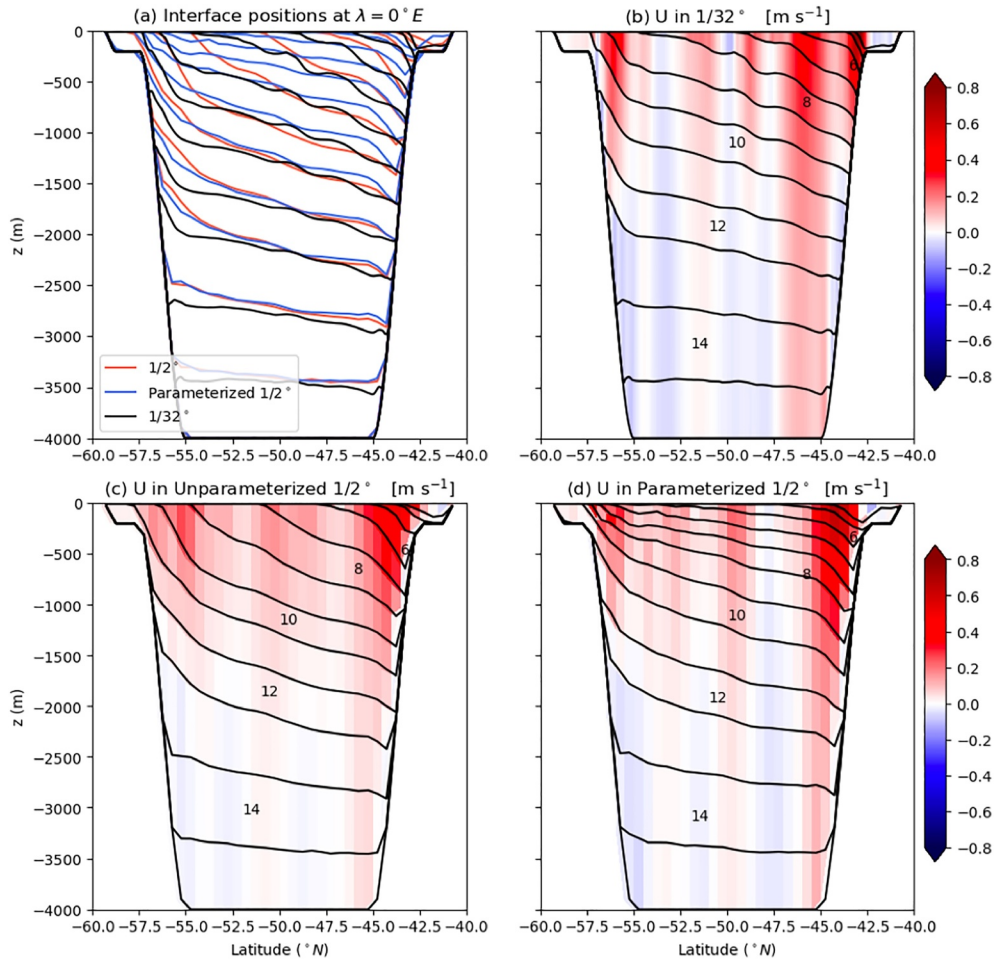

Figure 8. (a) Mean hydrography across the southern channel (Drake Passage) for the reference (1/32°) simulation, 1/2° simulation with no eddy parameterization, and 1/2° simulation with our backscatter scheme turned on. Hydrography is depicted as 500-day mean position of isopycnals. Time-mean zonal flow (contour interval of 0.05 m s^{-1}), with interface positions for the same three simulations, respectively, are shown in panels (b–d). This figure is based on Figure 8 of Marques et al. (2022).

Figure 6. The mean KE, which also shapes isopycnal structure through geostrophic balance, is best represented by our parameterized case. The unparameterized and Jansen et al. (2020) cases have KE values several orders of magnitude smaller in certain regions. We note that these cases also have KE structure characterized by unphysical zonal bands in the low latitudes. We hypothesize this is due to the deformation scale and fastest growing instability modes being poorly resolved at these latitudes, coupled with the relatively large choice of Smagorinsky viscosity leading to suppression of flow variability. The time-mean barotropic streamfuction, though less drastically than the KE, is also improved in our parameterized case relative to the reference. The improvement is particularly pronounced in the mid-latitude regions.

We next consider the density structure as a function of latitude. In Figure 7, meridional transects of 500-day averaged isopycnal positions are compared between the unparameterized, parameterized, and truth cases. The unparameterized case has overly steep isopycnals especially pronounced in the surface ocean. The locations of the isopycnal outcrops in the Southern Ocean are erroneous compared to the truth case, see the uppermost isopycnal in the bottom panel. In the case with our parameterization, the isopycnals are significantly closer to the reference solution. The slopes are aligned parallel with the reference and Southern Ocean ventilation is improved. However, there are still regions in which there are differences with the truth case, such as very low latitudes where eddy dynamics become less pronounced. Additionally, the North Atlantic region (middle panel) is slightly more stratified in the case with our parameterization compared to the reference.

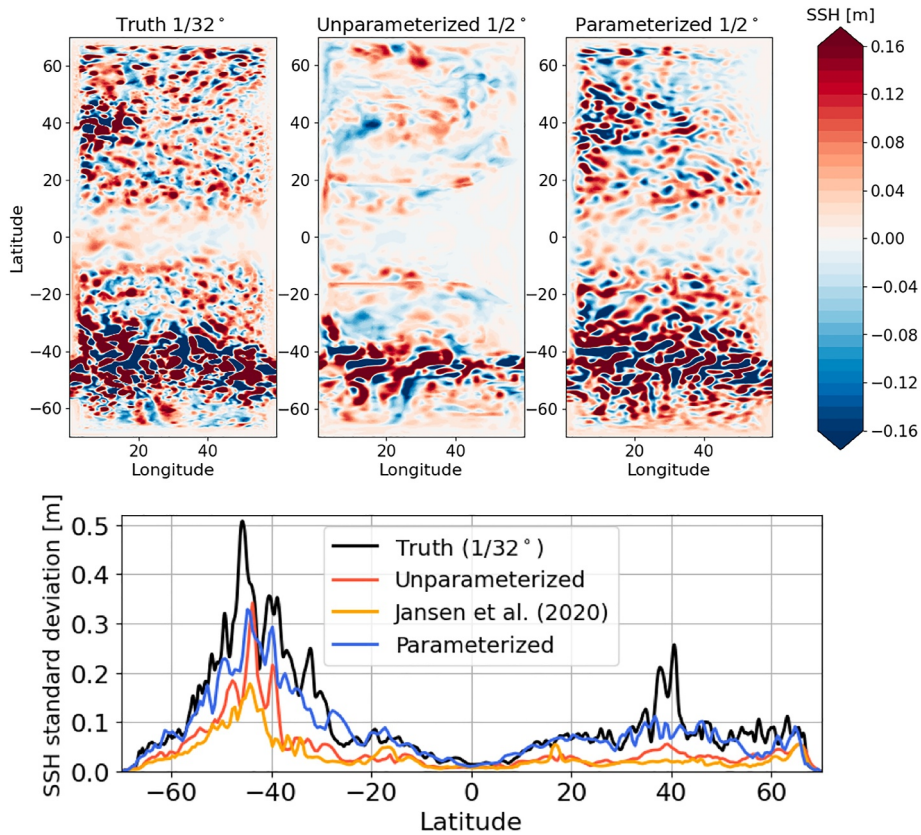

Figure 9. Upper row: 5-day averaged sea surface height (SSH) anomaly relative to a 500-day climatology for the reference (1/32°) simulation, 1/2° simulation with no eddy parameterization, and 1/2° simulation with our backscatter scheme turned on. Lower row: zonally averaged standard deviation of SSH computed for a 5-day averaged field for the same simulations and the Jansen et al. (2020) 1/2° case.

An additional transect through the southern channel (Drake Passage) is shown in Figure 8. Mean isopycnals are shown; although our parameterized case does not perfectly agree with the reference, there is an improvement compared to the overly steep isopycnals of the unparameterized case. The slight discrepancy is somewhat expected, as the idea of a single vertical structure being applicable to the entire ocean is not realistic. Even with the slight isopycnal deviations, the majority of the ocean has marked improvement with our scheme and the global APE is nearly identical to the reference. Time-mean zonal flow is also shown, indicating a vertical structure that is qualitatively similar between our parameterized and reference simulation. Further, the mean transport through Drake passage relative to the truth is most accurate in our parameterized case. The error is 11%, compared to 16% for the Jansen et al. (2020) case. Although improvement in isopycnal positions has been seen in simulations with GM, here we parameterize the buoyancy effects of eddies by using a kinetic energy backscatter alone. By energizing existing eddies in the flow in a physical manner, we are able to allow them to perform the extraction of APE from the large-scale flow without the need for an additional GM-like buoyancy closure at this resolution.

5.2. Influences on the Eddy Field

We next examine the influences of our scheme on eddy variability, energetics, and vertical structure. Having already shown substantial mean flow improvements, we note that these improvements stem from the more vigorous eddy field that our parameterization initiates. In Figure 9 we consider the field of the sea surface height (SSH) anomaly, where one may observe the eddy field. The truth and parameterized simulations show similar variability and structure across latitudes. The unparameterized case has much less variability, particularly in the meridional direction and in regions where the flow is less energetic. The standard deviation of SSH as a function of latitude also shows good agreement between the parameterized and truth cases. The Jansen et al. (2020) case, by contrast, has even less variability than the unparameterized case—emphasizing the problem of eddy-damping

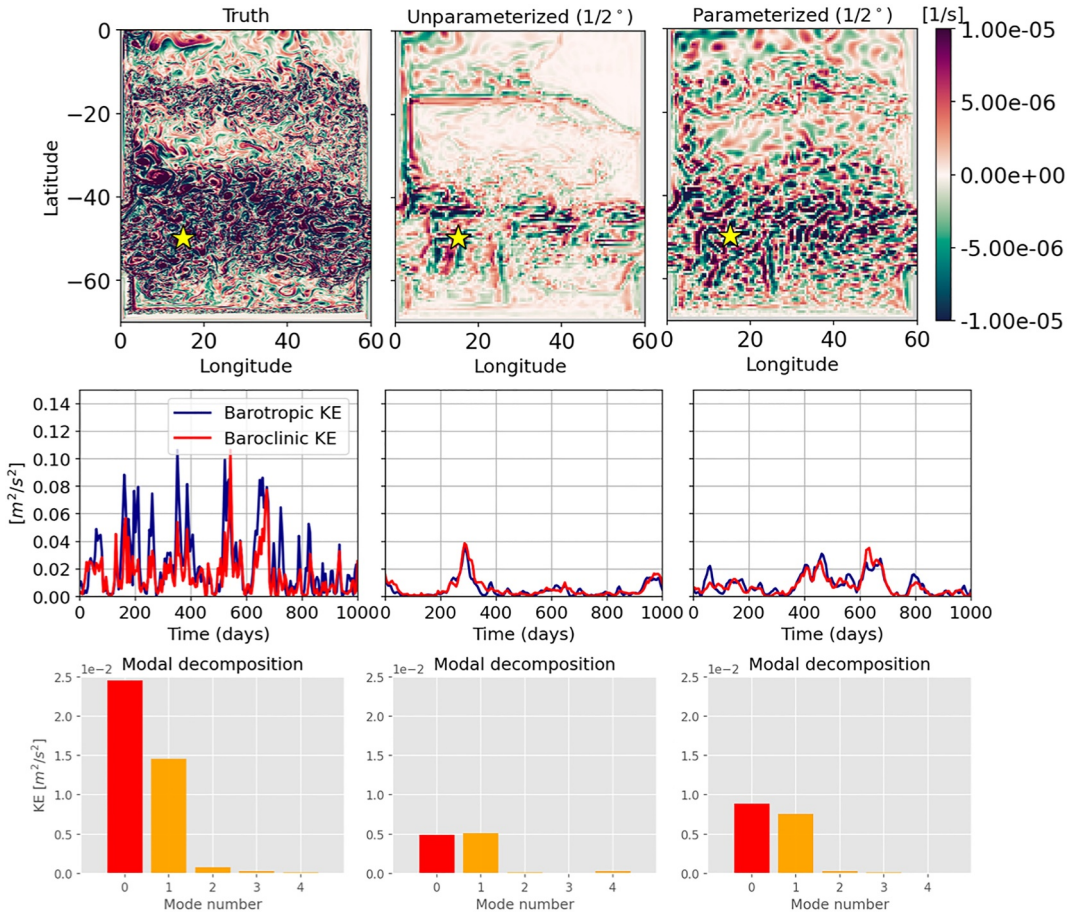

Figure 10. Left to right columns: Southern Ocean in the reference (1/32°) simulation, 1/2° case with no eddy parameterization, 1/2° case with our backscatter scheme. Top to bottom: 5-day averaged surface relative vorticity field, barotropic and baroclinic kinetic energy timeseries, and 500-day averaged decomposition of kinetic energy by vertical mode. The zeroth mode refers to the barotropic mode. In the latter two panels, we consider the starred point in the upper panel.

by GM and the inability of the backscatter to compensate. Thus, our backscatter scheme appears to be energizing eddies with appropriate surface scale and structure across latitudes.

We next consider the kinetic energy structure of the flow in greater detail. As shown in Yankovsky et al. (2022), one of the hallmarks of under-resolved eddies is energy trapping in the baroclinic vertical modes of the flow. Two locations—the northern hemisphere and the Southern Ocean—are examined in Figures 10 and 11. The relative vorticity fields at both locations are significantly improved between the cases without/with our parameterization turned on (relative to the 1/32° case). We then decompose the kinetic energy into its baroclinic and barotropic constituents and plot them as time series. In the ACC, there is a slight improvement in the energy level of both barotropic and baroclinic KE as well as variability. However, the eddies remain slightly less energetic, larger, and more sluggish in the parameterized run. A much more substantial improvement is evident in the northern hemisphere. Here, the time series show very similar temporal evolution and energy levels between our parameterized case and the truth. Finally, we consider the modal decomposition of the kinetic energy, by computing the vertical modes of the flow assuming flat bottom boundary conditions and plotting the kinetic energy associated with each vertical mode. As expected, the unparameterized case has a dominant energy component in the baroclinic part of the flow due to the unresolved vertical eddy fluxes and barotropization process at both locations. In the truth and parameterized case, we see a dominant part of the kinetic energy in the barotropic part of the flow. Note that some discrepancies arise; this is due to the fact that we are considering a point measurement which is very sensitive to individual eddy features passing through this location. For example, the northern hemisphere parameterized case has even more KE in the barotropic and baroclinic components than the truth. Taking a spatial average (not shown here) leads to better agreement. These results may be compared against an analogous analysis

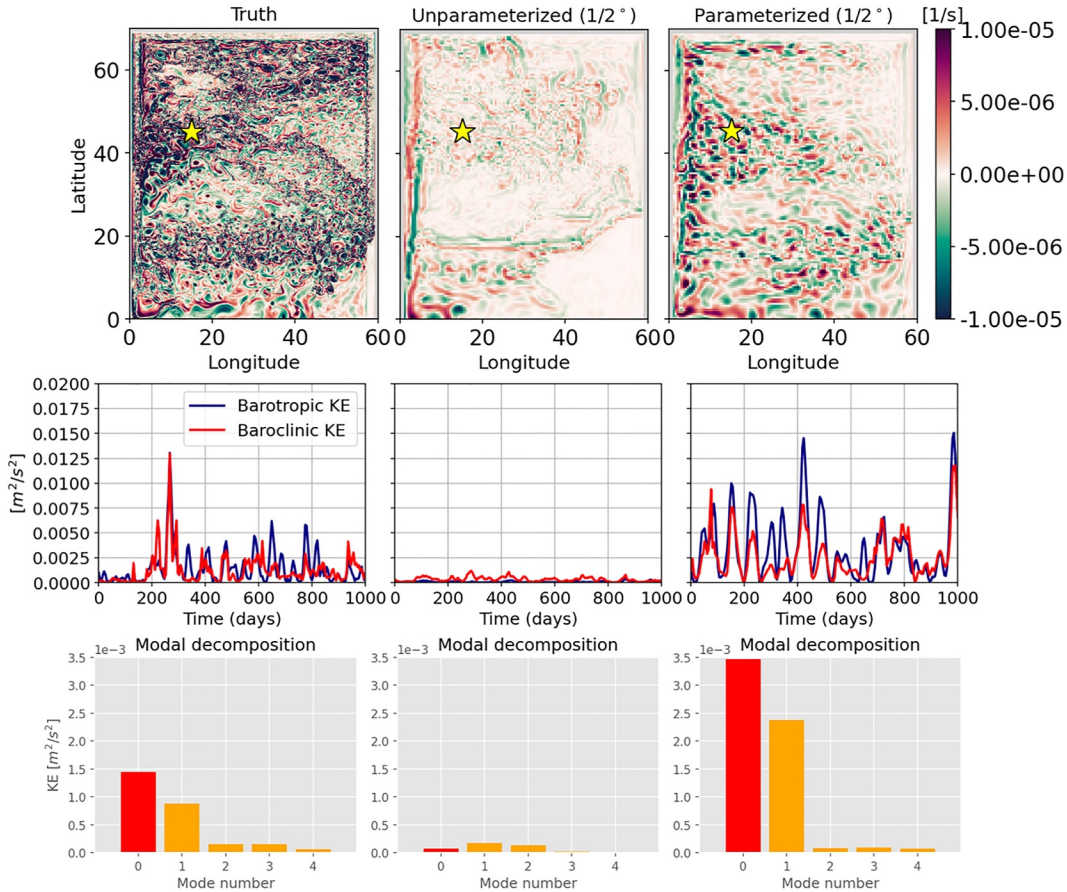

Figure 11. Same as in Figure 10, but for the northern hemisphere.

for various configurations of the Jansen et al. (2020) scheme in Figure 4; in the latter, the problem of under-barotropized and under-energized flow persists. We thus find that our parameterization represents the unresolved eddy influences on vertical structure in an appropriate way. We also emphasize that this is a 1/2° model that does not resolve the deformation scale at most latitudes. We cannot expect the eddy dynamics in the parameterized run to be perfectly in agreement with a 1/32° model, and they are not. Nonetheless, the parameterization offers significant improvements to barotropic and baroclinic KE levels, eddy vertical structure, and eddy influences on the mean flow (see prior subsection).

As an additional metric to assess the performance of our parameterization, we ask whether the eddies we energize through the kinetic energy backscatter are of a physical scale. We compute the energy-containing scale R_E (interpreted as the eddy scale) according to Thompson and Young (2006) using the field of the SSH anomaly (η_0') relative to a 500-day climatology as:

$$R_{\mathrm{E}} = \sqrt{\frac{\langle \eta_0'^2 \rangle}{\langle |\nabla \eta_0'|^2 \rangle}}, \tag{11}$$

where angle brackets denote time averaging over 500 days. In Figure 12 we compare R_E between the truth (1/32°), a 1/2° case with the Jansen et al. (2020) scheme turned on, and a 1/2° with our backscatter parameterization. For reference, the deformation scale is shown in black and the grid spacing in dashed gray. We see that the energy-containing scale for the case with our parameterization is relatively close to that of the truth case, and lies slightly above the grid scale. The Jansen et al. (2020) case has a significantly larger energy scale between 20°S and 40°S and the equatorial region. This result further adds validity to our backscatter approach—the eddies are growing to

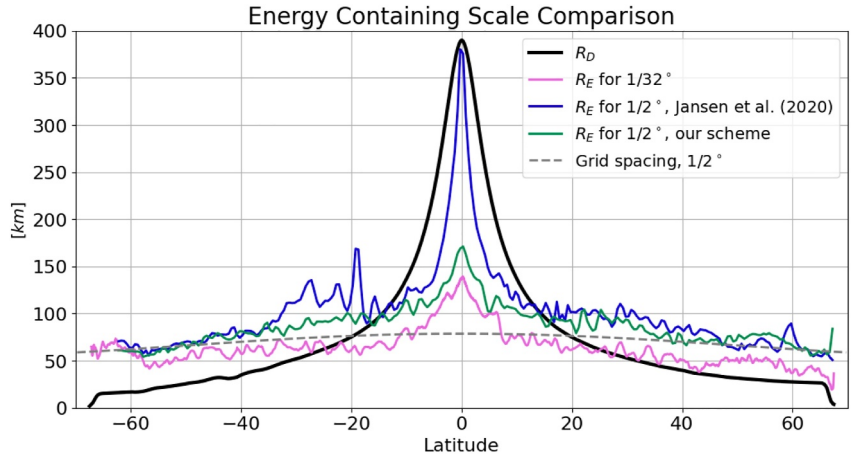

Figure 12. Zonally and 500-day averaged deformation scale (for 1/32° case) and energy-containing scale for the 1/32° case, 1/2° case with the Jansen et al. (2020) scheme, and our 1/2° backscatter case. Grid spacing for the 1/2° simulations is shown in dashed gray.

a reasonable size, following a physical dissipation pathway that arrests their growth, and impacting the mean flow in a manner consistent with our reference solution.

Finally, to gain a better understanding of the subgrid MEKE budget Equation 5, we consider plan-view plots of the constituent terms in Figure 13. We observe the highest subgrid MEKE values to occur in regions where the eddy activity is most vigorous and wind forcing is the highest, particularly the western boundary current region and Southern Ocean. The subgrid MEKE terms are primarily a balance between the backscatter and the biharmonic dissipation (the former is a sink of MEKE, the latter a source). The subgrid advection and frictional effects play a secondary role in the parameterization, being roughly an order of magnitude smaller. The dominance of backscatter and Smagorinsky viscosity terms brings up an interesting question: do we really need the MEKE budget? The advantage of MEKE is that it allows for time dependence in parameterizing the eddy energy fluxes, and one could argue that the advection and dissipation components are physically justified. On the other hand, we found over-dissipation through bottom drag when imposing vertical structures that were increasingly barotropic into the antiviscosity. It is possible that just by using the Smagorinsky viscosity and backscatter we could have a more simple and easily tunable parameterization. However, the balance between backscatter and viscosity may be particular to NW2, as the Smagorinsky viscosity coefficient used in this model is more than twice the standard value (Marques et al., 2022). We leave the question of whether a MEKE budget is necessary, and whether one can simply rely on backscatter and viscosity alone for future work.

6. Discussion

The development of this scheme has brought up new questions regarding its implementation in realistic climate models, use in conjunction with existing schemes, and next steps in its improvement. Here we discuss several such questions and offer some guidance for future work. Perhaps the most challenging next step is the implementation of our scheme into a more realistic, coupled climate model. We formulated our idealized NW2 model to specifically investigate mesoscale eddies and found that our parameterization captures their physics and influences on the mean flow at eddy-permitting resolutions. However, there is a well-known challenge in the modeling community: even if we recognize that a parameterization captures the relevant physics, there is no guarantee that it will improve the fidelity of a global climate model. There are interactions with other parameterizations, challenges with coupling, and compensating errors built into climate models through tuning that are impossible to foresee or predict a priori. Parameterization development has empirical elements and additional research will be required to successfully implement our scheme.

One of the main arguments we made here is that in NW2, we were able to parameterize both the kinetic and potential energy influences that eddies exert on the mean flow through the exclusive use of a kinetic energy backscatter. We argued that by energizing partially-resolved eddies, we facilitate the extraction of mean APE. Our findings confirm the well-established fact that GM in the eddy-permitting regime acts to damp eddies. However,

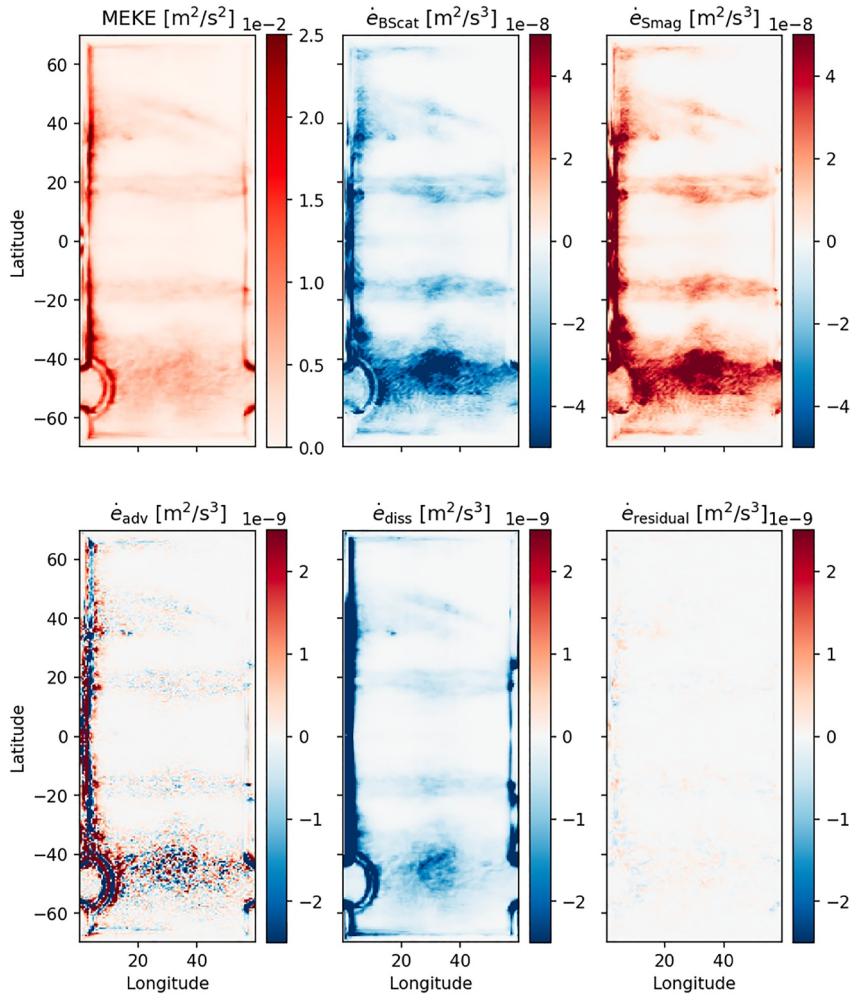

Figure 13. Subgrid mesoscale eddy kinetic energy (MEKE) computed from the MEKE budget and averaged over 500 days for the 1/2° case with our backscatter scheme (upper left), terms and residual (equivalent to time tendency) of the MEKE budget (other panels). Note that the Smagorinsky and backscatter terms are dominant, and have a colorbar scale 20 times that of the other terms.

we do encourage testing our backscatter alongside a GM configuration analogous to (Mak et al., 2023), where flow-splitting is performed and GM acts only on the large-scale part of the flow. Another promising idea is to employ an anisotropic form of GM (see R. D. Smith and McWilliams (2003), R. D. Smith and Gent (2004)). Past tests of this approach in a North Atlantic model with resolutions down to 0.1° have been shown to give energy levels comparable to runs without GM. Again, though we relied purely on backscatter, we acknowledge that this may pose challenges in a realistic climate model with varying degrees of eddy resolution as a function of latitude. A thoughtfully-applied GM version may be used in conjuction with our scheme to ideally constrain the isopycnal structure.

Another question that frequently arises in the parameterization literature is scale awareness. Our scheme is formulated specifically for the eddy-permitting regime, but is it scale aware within this regime? We have performed some preliminary tests by running a suite of NW2 simulations at 1/3° (not presented here) and 1/4° resolutions, with different tuning coefficient values. To first order, by linearly decreasing the magnitude of the tuning coefficient based on the resolution, we obtain scale awareness. The timeseries of KE and APE for the 1/4° simulations is shown in Figure 14. Based on the fact that a tuning coefficient of −1.0 was used at 1/2°, one would expect that at this doubled resolution the correct tuning coefficient would be around −0.5. Indeed, we see that when $c_{BScat} = -0.5$, the KE matches with the coarsened high-resolution result. The APE is also very close to the reference, although slightly low. This brings up an interesting point—the scale awareness of the vertical structure.

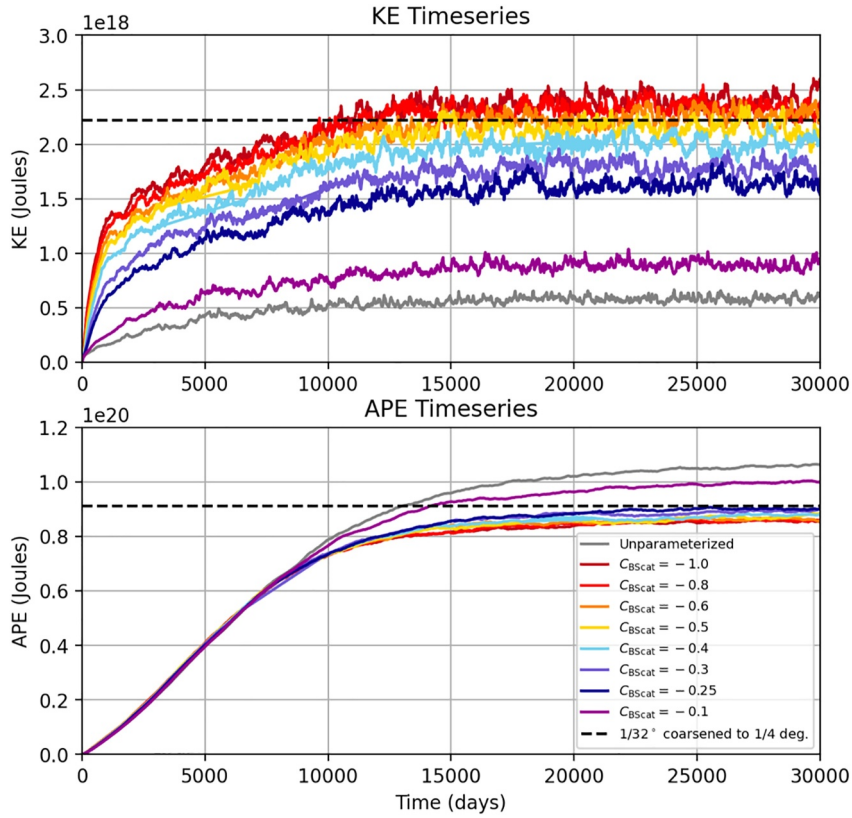

Figure 14. Timeseries of globally integrated kinetic and available potential energy for 1/4° simulations using our backscatter scheme, varying the tuning coefficient magnitude from 0.1 to 1.0. Also shown is the reference (1/32°) simulation's steady-state values coarsened onto a 1/4° grid.

Based on experiments testing various formulations of vertical structure, we find that an overly low APE (for the correct KE structure) occurs when the vertical structure does not decay sufficiently rapidly with depth, that is, the barotropic component is overly large. This means that at 1/4°, to have a better agreement with the APE of the reference simulation, we should make the backscatter slightly more surface-intensified. To this end, recent work by Zhang et al. (2024) suggests the possibility that a different modal structure, such as the surface quasi-geostrophic mode, may be used in place of the EBT mode. Informing the vertical structure based on flow dynamics and/or model resolution may prove to be an exciting avenue to pursue in further work.

7. Conclusions

We have presented a mesoscale eddy parameterization formulated as a momentum closure incorporating vertical structure into the parameterized fluxes. The parameterization relies on the mesoscale eddy kinetic energy (MEKE) budget framework, where a prognostic equation for eddy energy informs the backscatter magnitude. The backscatter is applied onto the equivalent barotropic (EBT) mode, which has a maximum near the surface and decays to zero near the bottom. Our scheme is aimed at representing both kinetic energy and potential energy influences of mesoscale eddies in the challenging eddy-permitting regime through the sole use of backscatter. We have tested the parameterization in the idealized NeverWorld2 model, at 1/2° and 1/4° resolutions. The results of the parameterized runs show that applying the backscatter to the EBT mode results in global kinetic and potential energies, isopycnal structure, and vertical energy partitioning that are consistent with a 1/32° reference simulation. By energizing the EBT mode we attempt to artificially mimic the end state of the eddy fluxes and interactions that give rise to an EBT vertical structure. Note that our backscatter scheme maintains the approach of using a 2D vertically averaged MEKE field, as in Jansen et al. (2015), unlike the approach proposed by Eden and Greatbatch (2008) and Juricke et al. (2019) of using a 3D EKE field. The 2D approach, while being

computationally less expensive, also bypasses the need to represent vertical eddy fluxes between layers, for which there is limited theoretical guidance.

An important aspect of our parameterization that requires some additional work is its scale awareness, and in particular how the scheme should be implemented in a realistic climate model that may range from eddy-permitting to non-eddying in various parts of the globe. As we emphasized in the introduction, our scheme specifically targets eddy-permitting resolutions where eddy features are already present in the flow; the objective is to reinforce them in a physical manner through backscatter rather than damping them through GM. The approach employed by Jansen et al. (2020) was to use a resolution function (as proposed by Hallberg (2013), but smooth rather than step-like in form) dependent on the deformation radius R_D as a scaling factor to mediate the backscatter and GM terms of the MEKE budget (Equation 5). When R_D is resolved, both the backscatter and GM terms are scaled to zero; when unresolved, they are scaled with equal magnitudes.

Based on our results, the scale-awareness approach of Jansen et al. (2020) does not appear to be the optimal choice. At coarse resolutions where eddies are not resolved, we suggest that backscatter be turned off entirely while GM serves as the dominant parameterization of eddy buoyancy effects. As the resolution increases and eddying features are increasingly permitted, backscatter magnitude should increase whereas GM should be diminished. At these resolutions GM damps the eddies that backscatter attempts to energize, and leads to double-counting of the APE removal—as we saw, properly energizing the partially-resolved eddies leads to APE removal without GM. Further, backscatter may yield beneficial results even when resolutions are around/just above the deformation scale. Thus, having an identical resolution function and coefficients for the GM and backscatter components is not recommended based on our results. Although developing the proper resolution function for backscatter and GM across all model resolutions is beyond the scope of this paper, we do encourage increased reliance on backscatter rather than GM at horizontal model resolutions of order R_D and finer. However, we also acknowledge that applying GM in an appropriate way—for instance, anisotropic GM or the splitting approach proposed by Mak et al. (2023)—may be explored alongside our scheme. Another avenue for future research that we did not consider in this study is how to approach isoneutral diffusion (Griffies et al., 1998; Redi, 1982).

This research provides valuable guidance for ocean modelers on how to parameterize mesoscale eddy effects in eddy-permitting regimes. The study opens new questions in how to best scale backscatter versus the Gent-McWilliams eddy parameterization component to ensure scale-awareness across all model resolutions. We also hope to build upon efforts of implementing backscatter in realistic ocean models (Chang et al., 2023) and investigate in greater depth how our parameterization performs in a fully coupled climate model.

Appendix A: Bounding the Viscous Coefficient Using Eddy Energy

Here we derive a theoretical upper bound for the backscatter antiviscosity, which we tested as an alternative formulation to the Jansen et al. (2020) scaling. The energy tendency of the viscous operator is given by

$$\mathcal{D} = \frac{1}{2}\boldsymbol{\sigma} : \dot{\mathbf{s}}, \tag{A1}$$

where under Reynolds averaging

$$\boldsymbol{\sigma} = \begin{bmatrix} \overline{u'u'} & \overline{u'v'} \\ \overline{u'v'} & \overline{v'v'} \end{bmatrix} \tag{A2}$$

is the Reynolds stress tensor and $\dot{\mathbf{s}}$ is the trace-free strain rate tensor defined in (Equation 2). Bars indicate time-averaged quantities and primes represent fluctuations. We will employ a standard harmonic eddy viscosity parameterization of the form

$$\boldsymbol{\sigma} = \boldsymbol{A} : \dot{\mathbf{s}}, \tag{A3}$$

where $\boldsymbol{A}$ is a fourth-order tensor satisfying the usual symmetries (e.g., R. D. Smith and McWilliams (2003)). We will assume a scalar viscosity, in which case (Equation A3) reduces to

$$\boldsymbol{\sigma} = \nu \dot{\mathbf{s}}. \tag{A4}$$

We seek to bound the magnitude of the coefficient ν. We start by employing the Cauchy-Schwartz inequality,

$$\left|\langle \boldsymbol{\sigma}, \dot{\mathbf{s}} \rangle\right| \leq \|\boldsymbol{\sigma}\| \|\dot{\mathbf{s}}\|, \tag{A5}$$

where $< \cdot >$ is the Frobenius/matrix inner product and $\|\cdot\|$ is the Frobenius norm. Substituting Equations A4 into A5, this becomes

$$\left|\langle \nu \dot{\mathbf{s}}, \dot{\mathbf{s}} \rangle\right| = |\nu| \|\dot{\mathbf{s}}\|^2 \tag{A6}$$

$$\leq \|\boldsymbol{\sigma}\| \|\dot{\mathbf{s}}\|, \tag{A7}$$

and so

$$|\nu| \leq \frac{\|\boldsymbol{\sigma}\|}{\|\dot{\mathbf{s}}\|}. \tag{A8}$$

We now seek a bound for $\|\boldsymbol{\sigma}\|$. By the definition of the Frobenius norm, we have

$$\|\boldsymbol{\sigma}\| = \left(\overline{u'^2}^2 + 2\overline{u'v'}^2 + \overline{v'^2}^2\right)^{1/2}, \tag{A9}$$

and by Hölder's inequality we have

$$\left(\int_S u'v' \, dx\right)^2 \leq \left(\int_S u'^2 \, dx\right)\left(\int_S v'^2 \, dx\right) \tag{A10}$$

for some measurable subset S of $\mathbb{R}^n$, wtih dx being an incremental measure in $\mathbb{R}^n$. If we define our averaging operator to be $\overline{(\cdot)} = \int_S (\cdot)\, dx$ we have

$$\overline{u'v'}^2 \leq \overline{u'^2}\,\overline{v'^2}. \tag{A11}$$

Defining the eddy kinetic energy $e = \frac{1}{2}(\overline{u'^2} + \overline{v'^2})$, we can substitute (Equation A11) into (Equation A9) to obtain the bound

$$\|\boldsymbol{\sigma}\| \leq \left(4K^2\right)^{1/2} = 2e. \tag{A12}$$

Finally, we can substitute (Equation A12) back into (Equation A8) to obtain the final bound,

$$|\nu| \leq \frac{2e}{\|\dot{\mathbf{s}}\|} = \frac{2e}{\left(\overline{u}_x^2 + \frac{1}{2}(\overline{v}_x + \overline{u}_y)^2 + \overline{v}_y^2\right)^{1/2}}. \tag{A13}$$

Note that this bound applies for both positive and negative ν, meaning it can be used to constrain both dissipation and backscatter coefficients.

Data Availability Statement

The Jupyter notebooks used to generate figures in the manuscript are available in a Zenodo repository at https://doi.org/10.5281/zenodo.8350252 (Yankovsky, 2023). We also include configuration files and 500 days of data for three 1/2° simulations presented in this manuscript—the case with no parameterization, the Jansen et al. (2020) scheme, and our new parameterization (see Sections 2 and 4). The NeverWorld2 configuration used

in this manuscript is detailed in Marques et al. (2022). The MOM6 source code and NeverWorld2 configuration files are available at https://doi.org/10.5281/zenodo.6993951 (Bhamidipati et al., 2022). The NeverWorld2 data set and detailed information on its contents are available at https://doi.org/10.26024/f130-ev71 (Marques, 2022).

Acknowledgments
The authors thank the members of the Ocean Transport and Eddy Energy Climate Process Team for insightful discussions, advice, and support throughout the course of this project. We are deeply grateful to Julian Mak, Peter Gent, and an anonymous reviewer for their thorough and helpful efforts in reviewing this manuscript. EY, KSS, and LZ were supported by NSF grant OCE 1912357 and NOAA CVP NA19OAR4310364. SB was supported by NSF grant OCE 1912420.

References

Bachman, S. D. (2019). The GM+E closure: A framework for coupling backscatter with the gent and McWilliams parameterization. *Ocean Modelling*, *136*, 85–106. https://doi.org/10.1016/j.ocemod.2019.02.006

Bhamidipati, N., Adcroft, A., Marques, G., & Abernathey, R. (2022). ocean-eddy-cpt/NeverWorld2: NeverWorld2-description-paper. *Zenodo [code]*. https://doi.org/10.5281/zenodo.6462289

Cessi, P. (2008). An energy-constrained parameterization of eddy buoyancy flux. *Journal of Physical Oceanography*, *38*(8), 1807–1819. https://doi.org/10.1175/2007JPO3812.1

Chang, C.-Y., Adcroft, A., Zanna, L., Hallberg, R., & Griffies, S. M. (2023). Remote versus local impacts of energy backscatter on the North Atlantic SST biases in a global ocean model. *Geophysical Research Letters*, *50*(21), e2023GL105757. https://doi.org/10.1029/2023GL105757

Chemke, R., & Kaspi, Y. (2016). The latitudinal dependence of the oceanic barotropic eddy kinetic energy and macroturbulence energy transport. *Geophysical Research Letters*, *43*(6), 2723–2731. https://doi.org/10.1002/2016GL067847

de La Lama, M. S., LaCasce, J. H., & Fuhr, H. K. (2016). The vertical structure of ocean eddies. *Dynamics and Statistics of the Climate System*, *1*(1), dzw001. https://doi.org/10.1093/climsys/dzw001

Delworth, T. L., Rosati, A., Anderson, W., Adcroft, A. J., Balaji, V., Benson, R., et al. (2012). Simulated climate and climate change in the GFDL CM2.5 high-resolution coupled climate model. *Journal of Climate*, *25*(8), 2755–2781. https://doi.org/10.1175/JCLI-D-11-00316.1

Eden, C., & Greatbatch, R. J. (2008). Towards a mesoscale eddy closure. *Ocean Modelling*, *20*(3), 223–239. https://doi.org/10.1016/j.ocemod.2007.09.002

Ferrari, R., Griffies, S. M., Nurser, A. J. G., & Vallis, G. K. (2010). A boundary-value problem for the parameterized mesoscale eddy transport. *Ocean Modelling*, *32*(3), 143–156. https://doi.org/10.1016/j.ocemod.2010.01.004

Ferreira, D., Marshall, J., & Heimbach, P. (2005). Estimating eddy stresses by fitting dynamics to observations using a residual-mean ocean circulation model and its adjoint. *Journal of Physical Oceanography*, *35*(10), 1891–1910. (Publisher: American Meteorological Society Section: Journal of Physical Oceanography). https://doi.org/10.1175/JPO2785.1

Fox-Kemper, B., Adcroft, A., Böning, C. W., Chassignet, E. P., Curchitser, E., Danabasoglu, G., et al. (2019). Challenges and prospects in ocean circulation models. *Frontiers in Marine Science*, *6*. https://doi.org/10.3389/fmars.2019.00065

Gent, P. R., & McWilliams, J. C. (1990). Isopycnal mixing in ocean circulation models. *Journal of Physical Oceanography*, *20*(1), 150–155. https://doi.org/10.1175/1520-0485(1990)020⟨0150:IMIOCM⟩2.0.CO;2

Gent, P. R., Willebrand, J., McDougall, T. J., & McWilliams, J. C. (1995). Parameterizing eddy-induced tracer transports in ocean circulation models. *Journal of Physical Oceanography*, *25*(4), 463–474. https://doi.org/10.1175/1520-0485(1995)025⟨0463:PEITTI⟩2.0.CO;2

Griffies, S. M. (2004). *Fundamentals of ocean climate models, Chapter 17*. Princeton University Press. https://doi.org/10.2307/j.ctv301gzg

Griffies, S. M., Gnanadesikan, A., Pacanowski, R. C., Larichev, V. D., Dukowicz, J. K., & Smith, R. D. (1998). Isoneutral diffusion in a z-coordinate ocean model. *Journal of Physical Oceanography*, *28*(5), 805–830. https://doi.org/10.1175/1520-0485(1998)028⟨0805:IDIAZC⟩2.0.CO;2

Griffies, S. M., & Hallberg, R. W. (2000). Biharmonic friction with a Smagorinsky-like viscosity for use in large-scale eddy-permitting ocean models. *Monthly Weather Review*, *128*(8), 2935–2946. https://doi.org/10.1175/1520-0493(2000)128⟨2935:BFWASL⟩2.0.CO;2

Griffies, S. M., Winton, M., Anderson, W. G., Benson, R., Delworth, T. L., Dufour, C. O., et al. (2015). Impacts on ocean heat from transient mesoscale eddies in a hierarchy of climate models. *Journal of Climate*, *28*(3), 952–977. https://doi.org/10.1175/JCLI-D-14-00353.1

Grooms, I., Majda, A. J., & Smith, K. S. (2015). Stochastic superparameterization in a quasigeostrophic model of the Antarctic circumpolar current. *Ocean Modelling*, *85*, 1–15. https://doi.org/10.1016/j.ocemod.2014.10.001

Hallberg, R. (2013). Using a resolution function to regulate parameterizations of oceanic mesoscale eddy effects. *Ocean Modelling*, *72*, 92–103. https://doi.org/10.1016/j.ocemod.2013.08.007

Henning, C. C., & Vallis, G. K. (2004). The effects of mesoscale eddies on the main subtropical thermocline. *Journal of Physical Oceanography*, *34*(11), 2428–2443. https://doi.org/10.1175/JPO2639.1

Hewitt, H. T., Roberts, M., Mathiot, P., Biastoch, A., Blockley, E., Chassignet, E. P., et al. (2020). Resolving and parameterising the ocean mesoscale in earth system models. *Current Climate Change Reports*, *6*(4), 137–152. https://doi.org/10.1007/s40641-020-00164-w

Jansen, M. F., Adcroft, A., Khani, S., & Kong, H. (2020). Toward an energetically consistent, resolution aware parameterization of ocean mesoscale eddies. *Journal of Advances in Modeling Earth Systems*, *11*(8), 2844–2860. https://doi.org/10.1029/2019MS001750

Jansen, M. F., & Held, I. M. (2014). Parameterizing subgrid-scale eddy effects using energetically consistent backscatter. *Ocean Modelling*, *80*, 36–48. https://doi.org/10.1016/j.ocemod.2014.06.002

Jansen, M. F., Held, I. M., Adcroft, A., & Hallberg, R. (2015). Energy budget-based backscatter in an eddy permitting primitive equation model. *Ocean Modelling*, *94*, 15–26. https://doi.org/10.1016/j.ocemod.2015.07.015

Juricke, S., Danilov, S., Koldunov, N., Oliver, M., Sein, D., Sidorenko, D., & Wang, Q. (2020). A kinematic kinetic energy backscatter parametrization: From implementation to global ocean simulations. *Journal of Advances in Modeling Earth Systems*, *12*. https://doi.org/10.1029/2020MS002175

Juricke, S., Danilov, S., Koldunov, N., Oliver, M., & Sidorenko, D. (2020). Ocean kinetic energy backscatter parametrization on unstructured grids: Impact on global eddy-permitting simulations. *Journal of Advances in Modeling Earth Systems*, *12*(1). https://doi.org/10.1029/2019MS001855

Juricke, S., Danilov, S., Kutsenko, A., & Oliver, M. (2019). Ocean kinetic energy backscatter parametrizations on unstructured grids: Impact on mesoscale turbulence in a channel. *Ocean Modelling*, *138*, 51–67. https://doi.org/10.1016/j.ocemod.2019.03.009

Khani, S., & Dawson, C. N. (2023). A gradient based subgrid-scale parameterization for ocean mesoscale eddies. *Journal of Advances in Modeling Earth Systems*, *15*(2). https://doi.org/10.1029/2022MS003356

Kitsios, V., Frederiksen, J. S., & Zidikheri, M. J. (2013). Scaling laws for parameterisations of subgrid eddy–eddy interactions in simulations of oceanic circulations. *Ocean Modelling*, *68*, 88–105. https://doi.org/10.1016/j.ocemod.2013.05.001

Kjellsson, J., & Zanna, L. (2017). The impact of horizontal resolution on energy transfers in global ocean models. *Fluids*, *2*(3), 45. https://doi.org/10.3390/fluids2030045

LaCasce, J. H. (2017). The prevalence of oceanic surface modes. *Geophysical Research Letters*, *44*(21), 11097–11105. https://doi.org/10.1002/2017GL075430

LaCasce, J. H., & Groeskamp, S. (2020). Baroclinic modes over rough bathymetry and the surface deformation radius. *Journal of Physical Oceanography*, *50*(10), 2835–2847. (Publisher: American Meteorological Society Section: Journal of Physical Oceanography). https://doi.org/10.1175/JPO-D-20-0055.1

Loose, N., Bachman, S., Grooms, I., & Jansen, M. (2022). Diagnosing scale-dependent energy cycles in a high-resolution isopycnal ocean model. *Journal of Physical Oceanography*, *53*(1), 157–176. https://doi.org/10.1175/JPO-D-22-0083.1

Mak, J., Maddison, J., Marshall, D., Ruan, X., Wang, Y., & Yeow, L. (2023). Scale-awareness in an eddy energy constrained mesoscale eddy parameterization. *Journal of Advances in Modeling Earth Systems*, *15*(12). https://doi.org/10.48550/arXiv.2306.08988

Mak, J., Maddison, J. R., Marshall, D. P., & Munday, D. R. (2018). Implementation of a geometrically informed and energetically constrained mesoscale eddy parameterization in an ocean circulation model. *Journal of Physical Oceanography*, *48*(10), 2363–2382. https://doi.org/10.1175/JPO-D-18-0017.1

Mak, J., Marshall, D. P., Madec, G., & Maddison, J. R. (2022). Acute sensitivity of global ocean circulation and heat content to eddy energy dissipation timescale. *Geophysical Research Letters*, *49*(8), e2021GL097259. https://doi.org/10.1029/2021GL097259

Marques, G. (2022). NeverWorld2 [Dataset]. *UCAR/NCAR - CISL - CDP*. https://doi.org/10.26024/F130-EV71

Marques, G., Loose, N., Yankovsky, E., Steinberg, J. M., Chang, C.-Y., Bhamidipati, N., et al. (2022). NeverWorld2: An idealized model hierarchy to investigate ocean mesoscale eddies across resolutions. *Geoscientific Model Development*, *15*(17), 6567–6579. https://doi.org/10.5194/gmd-15-6567-2022

Marshall, D. P., & Adcroft, A. J. (2010). Parameterization of ocean eddies: Potential vorticity mixing, energetics and Arnold's first stability theorem. *Ocean Modelling*, *32*(3), 188–204. https://doi.org/10.1016/j.ocemod.2010.02.001

Marshall, D. P., Maddison, J. R., & Berloff, P. S. (2012). A framework for parameterizing eddy potential vorticity fluxes. *Journal of Physical Oceanography*, *42*(4), 539–557. https://doi.org/10.1175/JPO-D-11-048.1

Porta Mana, P., & Zanna, L. (2014). Toward a stochastic parameterization of ocean mesoscale eddies. *Ocean Modelling*, *79*, 1–20. https://doi.org/10.1016/j.ocemod.2014.04.002

Redi, M. H. (1982). Oceanic isopycnal mixing by coordinate rotation. *Journal of Physical Oceanography*, *12*(10), 1154–1158. https://doi.org/10.1175/1520-0485(1982)012⟨1154:OIMBCR⟩2.0.CO;2

Smith, K. S., & Vallis, G. K. (2001). The scales and equilibration of midocean eddies: Freely evolving flow. *Journal of Physical Oceanography*, *31*(2), 554–571. https://doi.org/10.1175/1520-0485(2001)031⟨0554:TSAEOM⟩2.0.CO;2

Smith, K. S., & Vanneste, J. (2013). A surface-aware projection basis for quasigeostrophic flow. *Journal of Physical Oceanography*, *43*(3), 548–562. https://doi.org/10.1175/JPO-D-12-0107.1

Smith, R. D., & Gent, P. R. (2004). Anisotropic Gent–McWilliams parameterization for ocean models. *Journal of Physical Oceanography*, *34*(11), 2541–2564. (Publisher: American Meteorological Society Section: Journal of Physical Oceanography). https://doi.org/10.1175/JPO2613.1

Smith, R. D., & McWilliams, J. C. (2003). Anisotropic horizontal viscosity for ocean models. *Ocean Modelling*, *5*(2), 129–156. https://doi.org/10.1016/S1463-5003(02)00016-1

Thompson, A. F., & Young, W. R. (2006). Scaling baroclinic eddy fluxes: Vortices and energy balance. *Journal of Physical Oceanography*, *36*(4), 720–738. https://doi.org/10.1175/JPO2874.1

Yankovsky, E. (2023). Backscatter parameterization manuscript: Analysis notebooks and 1/2 degree simulation data. *Zenodo*. [code]. https://doi.org/10.5281/zenodo.8350252

Yankovsky, E., Zanna, L., & Smith, K. S. (2022). Influences of mesoscale ocean eddies on flow vertical structure in a resolution-based model hierarchy. *Journal of Advances in Modeling Earth Systems*, *14*(11), e2022MS003203. https://doi.org/10.1029/2022MS003203

Zhang, W., Griffies, S., Hallberg, R., Kuo, Y.-H., & Wolfe, C. (2024). The role of surface potential vorticity in the vertical structure of mesoscale eddies in wind-driven ocean circulations. *Journal of Physical Oceanography*, *54*(6), 1243–1266. https://doi.org/10.1175/JPO-D-23-0203.1

Zhang, W., & Wolfe, C. L. P. (2022). On the vertical structure of oceanic mesoscale tracer diffusivities. *Journal of Advances in Modeling Earth Systems*, *14*(6). https://doi.org/10.1029/2021MS002891